



Microscopic enrichment and porosity-permeability reduction mechanism of residual oil in tight sandstone reservoirs: an insight from Chang 8 Member, Yanchang Formation, Ordos Basin, China

Qianshan Zhou^{1,2,3} · Jiangyan Liu^{4,7} · Dongwei Zhang⁵ · Chao Li^{1,2} · Yueye Xiao^{1,2,6} · Guojun Chen^{1,2} · Chengfu Lyu^{1,2}

Received: 7 October 2023 / Accepted: 7 March 2024

© The Author(s) 2024

Abstract

This study delves into the micro-occurrence states and enrichment mechanisms of residual oil, pivotal for advancing the production from tight sandstone reservoirs, particularly from the Chang 8 Member of the Upper Triassic Yanchang Formation, Ordos Basin. Through an analysis of 23 core samples, employing high-pressure mercury injection, field emission scanning electron microscopy, thin section, and X-ray diffraction techniques, distinct reservoir types were categorized. The utilization of environmental scanning electron microscope, multi-solvent continuous extraction, and an oil components separation system facilitated an intricate analysis of residual oil micro-occurrence states and their subsequent effects on porosity and permeability reduction across varying reservoir types. The findings accentuate the integral role of reservoir type in determining residual oil distribution within tight sandstone reservoirs. Favorable pore throat sorting and connectivity in specified reservoir types are identified as conducive to residual oil enrichment with a higher concentration of light components. In contrast, elevated carbonatite and clay content in other reservoir types leads to adsorption of heavy components, disrupting pore throat connectivity, and impeding crude oil filling. The varied interactions between oil and rock, oil–oil, and pore throat sealing significantly impact the distribution of oil components of residual oil, culminating in a notable reduction of porosity and permeability by 2.63% and 0.197 mD, with corresponding reduction rates of 27.19% and 46.69%, respectively. The insights derived from this study furnish a theoretical foundation for augmenting tight oil recovery and comprehending the enrichment mechanism of residual oil driven by the heterogeneity of tight sandstone reservoirs.

Keywords Micro-occurrence states · Porosity and permeability reduction · Enrichment mechanism · Residual oil · Tight sandstone · Ordos Basin

Abbreviations

CEC Cation exchange capacity
DCM Dichloromethane
EDS Energy-dispersive spectrometry

FE-SEM Field Emission Scanning Electron Microscope
HPMI High-pressure mercury injection
mD Millidarcies
MeOH Methanol

✉ Dongwei Zhang
zdw.syky@sinopec.com

Chao Li
lichao@mails@lzb.ac.cn

¹ Northwest Institute of Eco-Environment and Resources, Chinese Academy of Sciences, Lanzhou 730000, Gansu, China

² Petroleum Resources Research, Gansu Province Key Laboratory, Lanzhou 730000, Gansu, China

³ National Engineering Research Center, Offshore Oil and Gas Exploration, Beijing 100028, China

⁴ Company National Engineering Laboratory for Exploration and Development of Low Permeability Oil & Gas Fields, PetroChina, Xi'an 710018, China

⁵ Petroleum Exploration and Production Research Institute, Sinopec, Beijing 102206, China

⁶ University of Chinese Academy Sciences, CAS, Beijing 100049, China

⁷ Present Address: Exploration and Development Research Institute of Changqing Oilfield Branch Company Ltd, PetroChina, Xi'an 710018, China

N ₂	Nitrogen gas
OMA	Oil-mineral aggregates
Rp1	The first peak
SARA-A	Aromatics
SARA-A	Asphaltenes
SARA-R	Resins
SARA-S	Saturates
THF	Tetrahydrofuran
TS	Thin Sections
UTW	Ultra-thin window
XRD	X-ray diffraction

Introduction

Tight sandstone reservoir has emerged as a significant focus in global unconventional oil exploration and development. It also stands as a critical unconventional resource, offering a notable alternative to conventional oil and gas, and facilitating the transition within the oil and gas sectors (Sun et al. 2019; Yang et al. 2023; Song et al. 2023). This oil type is closely associated with source rocks, undergoing in situ or short-distance migration and primarily accumulating in tight sandstone or limestone reservoirs (Yang et al. 2017). The Ordos Basin is a prominent tight oil distribution area, marking the first mature tight oil region to achieve industrialization in China.

As the global reserves of conventional oil and gas continue to decline, enhancing the recovery of tight oil becomes crucial for maintaining the equilibrium between oil and gas supply and demand. Previous research in tight oil reservoirs has explored various enhancement techniques, including horizontal drilling, water flooding, carbon dioxide flooding, and polymer flooding, to increase oil recovery rates (Strelets and Ilyin 2021; Song et al. 2022; Ren et al. 2023). Despite these efforts, the recovery rate from tight sandstone oil reservoirs remains under 10% (Liu et al. 2021), highlighting the pressing need for innovative enhanced oil recovery (EOR) strategies. In tight sandstone reservoirs, crude oil is classified into movable and residual categories. Movable oil refers to the crude that can be efficiently extracted using current development techniques, whereas residual oil is the portion that remains trapped within the reservoir's pore spaces after standard recovery or displacement procedures. Previous studies have shown that residual oil, including adsorbed oil, accounts for a significant portion of the oil in place, reaching up to 68% in tight sandstone reservoirs (Wang et al. 2018). This distribution of residual oil presents a considerable challenge in the development of oil fields.

Evaluation methods for residual oil, including adsorbed oil, are divided into direct and indirect approaches. Direct methods, such as the multi-solvent continuous displacement (or extraction) method, hierarchical crushing continuous

extraction method, multi-temperature pyrolysis, and techniques involving centrifugation and nuclear magnetic resonance, are effective in accurately determining the quantity and compositional variations of residual oil (Taheri-Shakib et al. 2019a, b; Pan and Liu 2009; Menhui et al. 2017; Huangfu et al. 2022; Xu et al. 2022). Indirect methods, including confocal laser scanning microscopy, environmental scanning electron microscopy, three-dimensional quantitative fluorescence, and micro-nano CT, provide valuable insights into the spatial distribution, location, and morphology of residual oil (Jin et al. 2022; Gong et al. 2015; Zhou et al. 2021, 2022b; Menhui et al. 2017, 2020; Guo et al. 2022; Xu et al. 2022). Understanding the occurrence state of residual oil requires a comprehensive analysis that includes its phase state, spatial distribution, morphology, quantity, and composition. Therefore, accurately identifying the presence, phase state, volume, and composition of tight oil, especially residual oil, in tight sandstone reservoirs is essential for formulating effective development strategies.

Tight sandstones are characterized by their pore throats, which range from the nanometer to micrometer scale, often exhibiting less than ideal connectivity (Li et al. 2018b). The presence of interstitial materials, primarily clay and carbonate, creates a complex pore and throat network, significantly increasing the heterogeneity of the reservoir (Qiao et al. 2020; Wang et al. 2020b; Er et al. 2022). Extensive research has focused on characterizing the pore structure (Lai et al. 2018; Liu et al. 2021), classifying and evaluating reservoir types (Zhengming et al. 2006; Qu et al. 2022), investigating the micro-occurrence states of tight oil (Gong et al. 2015; Xu et al. 2022; Zhou et al. 2022a, b), studying the mobility of tight oil and its influencing factors (Zhang et al. 2014; Jin et al. 2022), and exploring the distribution and potential extraction of residual oil (Yang et al. 2022; Baban et al. 2023). Despite these efforts, the relationship between the distribution of residual oil and the specific types of tight sandstone reservoirs has not been fully addressed, largely due to technical limitations that hinder the effective utilization of this resource. Consequently, a systematic analysis of the factors influencing different reservoir types is essential to fully understand the processes that lead to the enrichment of residual oil.

The accumulation of residual oil, including components such as adsorbed oil and asphaltene, plays a pivotal role in the migration and accumulation processes of crude oil, potentially altering the inherent properties and pore structure of reservoirs (Cai et al. 2010). Research focusing on the effects of asphaltene (including adsorbed oil and residual oil) on reducing pore and throat sizes primarily investigates: (1) its negative impact on porosity and permeability, as observed in core filling-displacement simulation experiments with different phases of crude oil (Taheri-Shakib et al. 2019a, b); (2) the impairment of reservoir permeability due to asphaltene

precipitation following carbon dioxide flooding (Bolouri and Ghodjani 2012; Mohammed et al. 2021); (3) the transformation of residual asphaltene caused by microbial degradation of crude oil within the reservoir (Davudov and Moghanloo 2019); and (4) the detrimental effects of heavy crude oil components, predominantly asphaltene, on reservoir permeability as determined through numerical simulation experiments (Alimohammadi et al. 2019; Davudov and Moghanloo 2019). Despite these insights, there remains a significant gap in research under real geological conditions regarding the interaction between residual tight oil's response in the reservoir and the decrease in porosity and permeability across various reservoir types, especially from the perspective of rock–fluid interaction. The mechanisms driving the enrichment of residual oil and its subsequent impact on reservoir quality are critical areas that require further exploration in both existing literature and future studies. Elucidating these mechanisms will provide a direct theoretical basis for understanding the influence of residual oil (including adsorbed oil, asphaltene, etc.) on pore and throat diminution in tight sandstone reservoirs.

In this investigation, we introduce a novel characterization approach that synergizes direct (specifically, multi-solvent continuous extraction) and indirect (via Environmental Scanning Electron Microscopy) techniques to elucidate the intricate micro-occurrence states of residual oil within tight sandstone reservoirs. This methodology distinguishes itself from previous studies by leveraging a refined classification system for reservoir types, aiming to uncover the nuanced microscopic mechanisms that govern the enrichment of residual oil and its consequential impacts on reservoir porosity and permeability. Our focused exploration spans the quantitative delineation of residual oil, its spatial distribution, and the resultant effects on reservoir characteristics, anchored in oil–rock interaction insights. This concise approach underscores the novelty of our research, setting a new benchmark for enhancing tight oil recovery and understanding residual oil's complex enrichment within the heterogeneous landscape of tight sandstone reservoirs.

Geological settings

The Ordos Basin is the second-largest sedimentary basin in China, encompassing an area of 25×10^4 km² (Song et al. 2023; Yang et al. 2023). The periphery of the basin exhibits substantial deformation, while its core maintains a simplistic structure. The basin's western region is characterized by a gentle, extensive monoclinic dip, with an overall dip angle of less than 1° (Liu et al. 2021). Taking into account the bedrock depth, the current structural layout, and the historical tectonic evolution, the basin has been divided into

six secondary tectonic units, as depicted in Fig. 1a: Yishan Slope, Western Margin Thrust Zone, Jinxi Flexure Zone, Tianhuan Depression, Yimeng Uplift, and Weibei Uplift (Li et al. 2018a, b).

The Ordos Basin's tectonic evolution, initially part of the North China Craton's passive margin during the Paleozoic era, underwent significant transitions due to the collision between the North China and Yangtze cratons in the Mesozoic. This collision catalyzed the development of fluvial and lacustrine environments, alongside the accumulation of Jurassic coal-bearing sequences under humid conditions, indicative of the basin's complex subsidence history and favorable sedimentary conditions for hydrocarbon generation (Yang et al. 2017). The Cenozoic era, marked by the uplift of adjacent mountain ranges due to the India-Asia collision, introduced arid conditions and led to the deposition of continental clastic sediments, further shaping the basin's stratigraphy and influencing its hydrocarbon systems (Zhou et al. 2022b). The structural integrity of the basin, relatively stable despite surrounding orogenic compressions, created conducive environments for structural traps and affected the maturation and migration pathways of organic matter, emphasizing the Ordos Basin's significant hydrocarbon potential amidst its dynamic geological history (Sun et al. 2019). This intricate interplay between geological processes and sedimentary environments underscores the Ordos Basin's critical role in China's oil and gas exploration endeavors.

Based on the characteristics of sequence stratigraphy, the Yanchang Formation is divided into ten distinct oil-bearing layers, labeled from Chang 10 to Chang 1, in ascending order (refer to Fig. 1b). The sedimentary and tectonic evolution of the Yanchang Formation can be segmented into three main phases: (1) The phase from Chang 10 to Chang 7 is characterized by a lake transgression phase, which marks the transition from the lake's formation to its expansion. The initial deposits consist of gray–green massive feldspathic sandstone, which gradually transitions to gray–green and gray–black mudstone, with a total sedimentary thickness ranging from 100 to 300 ms. (2) The Chang 7 phase signifies the peak of the lake basin, leading to extensive deposits of dark mudstone and oil shale within shallow to semi-deep lake facies. This phase covers a sedimentary area of 10×10^4 km². (3) The interval from Chang 6 to Chang 1 marks the delta construction phase of the lake basin. As the lake waters recede and eventually disappear, the sedimentary sequence transitions from gray–green medium to fine-grained sandstone to mudstone and coal measures, with an overall thickness of 350 to 500 ms. Notably, the Chang 8 oil layer is identified as a key horizon for unconventional oil and gas exploration and development in the Ordos Basin.

The Chang 8 reservoir in the Ordos Basin is primarily characterized by a sedimentary delta system in both the

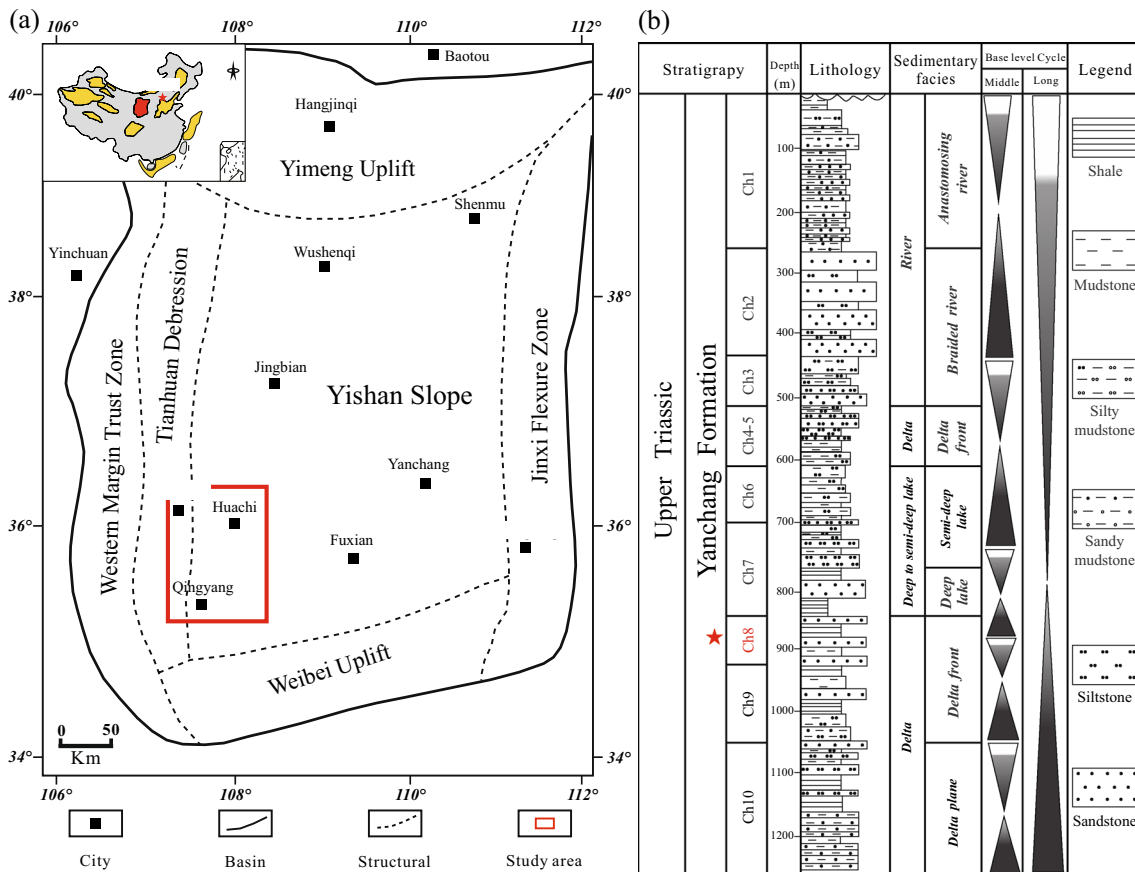


Fig. 1 a Location and tectonic units of the Ordos Basin; b Stratigraphic columns and depositional environment of the Yanchang Formation

southwest and northeast regions. In particular, the Chang 8 tight sandstone reservoirs in the Huaqing area are predominantly influenced by braided river delta depositional processes (Yao et al. 2013). These reservoirs are mainly composed of lithic arkose and feldspathic litharenite sandstones (Baoquan et al. 2021). Within the reservoir, sediment sorting varies from good to medium, and the particle roundness is mostly subangular. The grain-support structure is largely defined by point-line contacts, suggesting a medium level of structural maturity. Drilling data indicate that the Chang 8 reservoir generally contains oil, although it is characterized by low porosity (with an average of 8.27%) and ultra-low permeability (with an average of $0.51 \times 10^{-3} \mu\text{m}^2$).

Methodology

Sampling procedures

In this study, 23 tight sandstone samples were collected from the Huaqing area of the Ordos Basin, specifically from the Chang 8 Member of the Upper Triassic Yanchang Formation. These samples were extracted from depths ranging

between 1956 and 2200 ms. Notably, the chosen sampling locations primarily covered the underwater distributary channel microfacies, an area distinguished by superior physical properties and a high density of oil resources within the region. The following sections will elaborate on the process of sample preparation and the analytical methods employed in the study:

The tight sandstone samples collected were initially mounted on a drilling machine to produce standard cylindrical specimens with a diameter of 2.5 cm, with the specific details of these specimens documented in Table 1. Additionally, fresh samples measuring 1 cm × 1 cm were carefully chiseled from each specimen. The remaining material was then reduced to the smallest pieces achievable. Subsequently, all obtained samples were placed in an oven set at 100 °C and dried for a continuous period of three days to remove any moisture absorbed during the preparation stage. The process concluded with the production of approximately 10 g of sandstone particles, all of which had a particle size of less than 200 mesh. All samples were encased in filter paper and placed into a Soxhlet Extractor. For the extraction process, a solvent mixture of dichloromethane (DCM) and methanol (MeOH) (DCM: MeOH = 9:1 v/v) was employed,

Table 1 Multi-solvent continuous extraction data and basic sample information

Samples	D (m)	L (cm)	Φ (cm)	V (cm ³)	Before extraction					After extraction				
					P_v (cm ³)	Por (%)	Per (mD)	ρ (g/cm ³)	W g	P_v (cm ³)	Por (%)	Per (mD)	ρ (g/cm ³)	W (g)
S1	2148.6	3.889	2.513	19.282	2.183	11.32	1.320	2.291	44.184	3.045	15.79	1.857	2.254	43.458
S2	2138.1	3.914	2.504	19.276	2.099	10.89	0.860	2.287	44.086	2.969	15.40	1.250	2.252	43.406
S3	2147.9	3.677	2.508	18.170	2.286	12.58	2.850	2.251	40.903	3.056	16.82	3.380	2.214	40.233
S4	2149.5	3.897	2.513	19.332	2.219	11.48	2.327	2.247	43.444	3.170	16.40	2.830	2.209	42.706
S5	2191.3	3.922	2.500	19.257	1.899	9.86	0.937	2.290	44.093	2.735	14.20	1.480	2.254	43.398
S6	2193.2	3.994	2.501	19.625	1.837	9.36	0.463	2.306	45.260	2.551	13.00	0.754	2.276	44.662
S7	2242.4	3.975	2.501	19.533	1.992	10.20	0.406	2.344	45.783	2.592	13.27	0.556	2.316	45.229
S8	2188.0	4.109	2.508	20.298	1.851	9.12	0.460	2.410	48.914	2.365	11.65	0.524	2.386	48.422
S9	2287.5	4.034	2.520	20.118	1.986	9.87	0.352	2.313	46.533	2.531	12.58	0.568	2.288	46.028
S10	2134.2	3.882	2.498	19.030	1.972	10.36	0.474	2.314	44.028	2.603	13.68	0.725	2.284	43.474
S11	2062.2	3.960	2.485	19.213	1.600	8.33	0.520	2.384	45.801	2.148	11.18	0.740	2.359	45.332
S12	2228.3	3.939	2.502	19.368	1.487	7.68	0.340	2.315	44.844	2.049	10.58	0.430	2.292	44.382
S13	2239.7	3.968	2.377	17.613	1.809	10.27	0.076	2.359	41.550	2.258	12.82	0.100	2.336	41.144
S14	2192.6	4.154	2.517	20.668	1.699	8.22	0.349	2.348	48.522	2.289	11.08	0.521	2.322	47.996
S15	2168.5	3.265	2.505	16.097	1.658	10.30	0.105	2.413	38.839	1.813	11.26	0.231	2.401	38.656
S16	2288.6	3.991	2.519	19.891	2.011	10.11	0.261	2.296	45.672	2.532	12.73	0.400	2.269	45.133
S17	2235.6	3.885	2.510	19.225	1.821	9.47	0.089	2.380	45.752	2.176	11.32	0.110	2.360	45.362
S18	1956.3	3.782	2.510	18.714	1.890	10.10	0.130	2.427	45.409	2.130	11.38	0.167	2.414	45.183
S19	2296.2	4.421	2.499	21.688	1.308	6.03	0.140	2.324	50.414	1.555	7.17	0.257	2.314	50.194
S20	2238.2	4.054	2.510	20.065	1.256	6.26	0.025	2.398	48.106	1.437	7.16	0.038	2.388	47.908
S21	2163.8	3.905	2.497	19.124	1.480	7.74	0.094	2.461	47.058	1.706	8.92	0.121	2.450	46.862
S22	2546.3	3.409	2.488	16.580	1.275	7.69	0.068	2.292	37.996	1.409	8.50	0.116	2.283	37.843
S23	2144.4	3.97	2.510	19.644	1.733	8.82	0.052	2.426	47.655	1.898	9.66	0.079	2.415	47.449

D: Depth; L: Length; Φ : Diameter; V: Volume; P_v : Pore volume; Por: Porosity; Per: Permeability; ρ : Density; W: Weight

continuously circulating through the system (Menhui et al. 2017; Zhou et al. 2022a, b). It is crucial to highlight that all chemicals used were subject to distillation purification before their application. The solvent was refreshed every two days until it remained colorless, signifying the thorough removal of free oil from the samples. Both the columnar sample and the 1 cm \times 1 cm block sample were dried in an oven set at 70 °C for two days to remove any residual organic solvents. After being allowed to cool to room temperature, the block sample was subjected to investigate the micro-level presence of residual oil. The initial weight of the sample was meticulously recorded, after which its diameter and length were accurately measured using a vernier caliper. These measurements facilitated the calculation of the sample's apparent volume, which in turn allowed for the subsequent evaluations of porosity and permeability. Following the initial procedures, the column samples, along with all other remaining samples, were wrapped in filter paper and placed in a Soxhlet extractor. The extraction process utilized a mixed solvent

composed of DCM, *tetrahydrofuran* (THF), and MeOH in a volume ratio of DCM:THF:MeOH = 50:25:25. After the extraction, the samples were dried in an oven set at 70 °C and then allowed to cool to room temperature for further analysis. Concurrently, the solution obtained from the column samples was reduced in volume to concentrate the oil components for analysis. Block samples with dimensions of 1 cm \times 1 cm were meticulously prepared into *thin sections* (TS) and subsequently analyzed using a *field emission scanning electron microscope* (FE-SEM). This process was undertaken for the detailed observation and identification of the samples' microstructural characteristics. The column samples were accurately weighed prior to conducting tests to assess their porosity and permeability. Following these measurements, calculations were executed to ascertain the influence of residual oil reduction on these critical properties. The analytical process culminated with *high-pressure mercury injection* (HPMI) testing performed on the column samples, aimed at evaluating their pore structure and

distribution. Following the extraction with organic reagents, samples with a particle size of less than 200 mesh were analyzed to determine their mineral compositions using the *X-ray diffraction* (XRD) method. This technique allowed for the precise identification and quantification of the mineral-ogical constituents present in the samples.

Analytical methods

Mineral composition

XRD is recognized as the most direct, dependable, and mature method for analyzing rock mineral compositions (Wang et al. 2020a). In this investigation, the samples were prepared through an extraction process using a solvent mixture of DCM, THF, and MeOH, in a volume ratio of 50:25:25. This preparation ensured the samples met the requirements for fluorescence level 4 and below, a prerequisite for quantitative mineral analysis (Huangfu et al. 2022). The XRD analysis was conducted with a *Rigaku Ultima IV* (Japan), featuring a 3 kW Cu Ka X-ray source and a 285 mm angle measuring device, capable of spanning measurement angles from -110° to 180° . This configuration guaranteed a precision exceeding $\pm 0.02^{\circ}$ and a stability better than $\pm 0.002^{\circ}$. Operating at a voltage of 40 kV and a current of 150 mA, the instrument supported a scanning speed of 2° (2θ)/min, a data acquisition step width of 0.02° (2θ), and a scan range from 2.6° to 45° . Upon completion of the analysis, the mineral compositions of the rocks were determined based on the diffraction spectra, with a testing error margin kept below $\pm 2\%$.

Pore types and pore sizes

TS and FE-SEM played a pivotal role in identifying pore types in this research. Utilizing a polarizing microscope, it was possible to observe and differentiate various characteristics of the casting thin sections, including support type, particle contact mode, particle size, sorting, presence of grinding circles, and microstructure. Thin sections provide a clear visualization of the reservoir space, proving to be an invaluable tool for examining the distribution characteristics of reservoir pores (Liu et al. 2021). Observations of TS were carried out using a *Zeiss* microscope manufactured in Germany. The identification of components was mainly based on the recognition of debris particles, while pore types were determined through the application of alizarin red staining. For each sample, more than 20 fields of view were analyzed, utilizing both TS and FE-SEM images.

The FE-SEM facilitates ultra-high-resolution observation of microstructures, while *X-ray energy-dispersive spectrometry* (EDS) aids in identifying mineral compositions. Following the extraction with organic reagents to eliminate

residual oil, the samples were subjected to argon ion polishing to prepare them for micro-nano pore examination in the sandstone samples. These observations were conducted under controlled environmental conditions, specifically at 35% air humidity and 20°C . The experimental apparatus included a *Merlin* compact FE-SEM, which was paired with an X flash/30 X-ray spectrometer and a 685°C argon ion polishing system. The instrumental settings were optimized for detailed analysis, with an accelerating voltage range of 20 V to 30 kV, a magnification spectrum from $12\times$ to $2000000\times$, and achieving a resolution of 0.8 nm at 15 kV. Pore size determination was carried out using *Nano Measurer* v1.2 software. After calibrating the scale, individual pores in each image were meticulously measured, allowing for the calculation of the corresponding pore size based on the identified pore type.

Porosity and permeability

The porosity and permeability of the tight sandstone reservoirs being studied were assessed using the PoroPDP-200, an automated overburden porosity and permeability measurement instrument provided by an American core analysis company. In compliance with the API RP-40 standard for rock porosity and permeability measurement established by the American Petroleum Institute, this instrument is recognized as a gold standard in the international evaluation of rock porosity and permeability. It is capable of measuring porosity in a range from 0.01 to 40%, and its permeability detection capabilities extend from 0.00001 to 10 mD.

The instrument's software employs Boyle's law to calculate porosity, using helium gas with a purity of 99.99% for porosity measurements at a pressure under 0.7 MPa. Although the steady-state method is widely used for measuring apparent permeability, the unsteady-state approach, or the pressure pulse decay method, provides significant advantages when analyzing low-permeability media (Yang et al. 2019). Therefore, the apparent permeability of the tight sandstone samples was determined using the pressure pulse decay method, employing non-adsorbed nitrogen gas (N_2). To ensure that temperature fluctuations did not impact the results, the entire setup—except for the computer and gas cylinder—was placed within a temperature-controlled enclosure maintained at 22°C . The system then automatically calculates the permeability data, offering precise and reliable measurements essential for understanding the flow characteristics of tight sandstone reservoirs.

Pore structure

HPMI experiments have been established as a fundamental technique for detailing the pore structure and throat

distribution within reservoirs (Liu et al. 2021). In the current investigation, columnar samples, following extraction with organic reagents and having known parameters such as pore volume, porosity, permeability, and rock density, underwent analysis using the *AutoPore IV 9510* mercury intrusion meter. This instrument is capable of exerting a maximum pressure of 414 MPa and features a pore aperture detection range from 30 Å to 1000 µm. The automated post-test analysis by the instrument's computer software provides an extensive set of pore structure metrics. These include maximum mercury saturation, extrusion efficiency, displacement pressure, capillary median pressure, peak pore throat radius, mean throat radius, structure coefficient, and throat sorting coefficient. Collectively, these measurements effectively fulfill the analytical needs for characterizing the intricate pore architecture of tight sandstone reservoirs.

Micromorphology observation

Over the past two decades, ESEM has become an essential technique for exploring the micro-occurrence states of crude oil, as evidenced by numerous studies (Gong et al. 2015; Zhou et al. 2021, 2022b). ESEM enables the detailed observation of micro-to-nano scale pore throat morphology and the intrinsic characteristics of fluids under conditions of low vacuum. When combined with EDS, this method leverages the unique X-ray photon energies emitted by different elements to quantitatively analyze the carbon content in hydrocarbons. This synergistic approach allows for both qualitative and quantitative assessments of oil content within rock samples and on the surfaces of minerals (Gong et al. 2015; Zhou et al. 2021, 2022b).

The experiments utilized the *Quanta FEG450* ESEM, which is integrated with an EDS system. Measurements were carried out in the ambient low vacuum mode, with the vacuum degree within the sample chamber maintained at 0.08 mbar. The operational settings were configured at a working voltage of 10 kV, a current of 10 mA, and a beam current of 213.2 µA. This instrument facilitates a 100 mm range of movement for samples both vertically and horizontally, and operates at a temperature of 21 °C. The spectrometer is equipped with an ultra-thin window (UTW) detector, which efficiently detects elements with atomic numbers ranging from 4 (Beryllium, Be) to 92 (Uranium, U), with a detection error margin below ±3%. To improve sample conductivity and reduce the errors commonly associated with traditional carbon sputtering techniques, samples underwent a preparatory step of 30-second platinum target gold plating prior to the examination.

Soxhlet extraction

The experiment utilized a *Soxhlet Extractor*, employing distillation-purified reagents such as DCM, THF, and MeOH in a specified ratio (DCM:THF:MeOH = 50:25:25 v/v/v). Before initiating the experiment, the filter paper encasing the sample underwent a pre-extraction process with DCM until it turned colorless, ensuring the removal of any soluble impurities. Additionally, both the filter cartridge and the extractor were meticulously cleaned with DCM to eliminate potential contaminants. For the experiment, tight sandstone samples were wrapped in the pre-treated filter paper, accurately weighed, and then placed in the sample chamber. The apparatus was carefully assembled, and the solvent mixture was introduced into the chamber, followed by 2–3 reflux cycles to maintain the solvent volume between half and two-thirds of the bottom flask's capacity. The thermostatic heating sleeve was then activated to a temperature of 55 °C to facilitate the extraction process. To ensure optimal extraction efficiency, the solvent level was regularly monitored and replenished to keep it above half of the bottom flask's volume throughout the heating phase. The solvent was replaced daily until it remained colorless after the final extraction cycle, indicating the complete removal of extractable organic material, a process that typically lasted between 3–5 days. Upon the conclusion of the extraction phase, the sample was removed and placed in a constant-temperature drying oven set at 70 °C to eliminate any residual solvent. The difference in mass before and after the experiment provided the weight of the extracted substances, offering insights into the organic content of the tight sandstone samples.

Separation of family components

The analysis of petroleum constituents within rock sample extracts involves a methodical process that starts with the dissolution of the extract in chloroform. After filtration, the solution is evaporated to dryness at temperatures below 40 °C. The procedure for separating the petroleum constituents into saturates, aromatics, resins, and asphaltenes involves several carefully controlled steps: ① Dissolution and Filtration: The initial extract from the rock sample is dissolved in chloroform. Following filtration, the solution is evaporated under conditions that ensure no temperature exceeds 40 °C. ② Asphaltene Precipitation: A precise amount of the dry extract, ranging from 15 to 50 mg, is weighed and treated with about 30 mL of *n*-hexane, followed by ultrasonic dissolution to enhance mixing. This mixture is left to stand for 12 h, allowing for the complete precipitation of asphaltenes. The precipitated asphaltenes are collected in a tare-weighted bottle. ③ Saturate Separation: Saturates are leached from the filtrate using *n*-hexane in

3–5 mL increments, adding up to approximately 30 mL in total. This gradual leaching process employs a tare-weighted bottle to collect the saturates, ensuring constant weight. ④Aromatic Hydrocarbons Separation: Aromatic hydrocarbons are separated through a similar leaching process using *dichloromethane*, also in 3–5 mL increments to reach a total of about 30 mL. A tare-weighted bottle is used for collection to maintain consistent weight. ⑤Resin Separation: The separation of resins is facilitated by employing 10 mL of anhydrous ethanol followed by approximately 10 mL of chloroform for leaching. A tare-weighted bottle collects the resins, ensuring the process's integrity by maintaining consistent measurement conditions. ⑥Evaporation and Weight Calculation: The collected fractions of saturates and aromatics are evaporated to dryness at temperatures maintained below 40 °C, whereas the resins and asphaltenes are handled at temperatures below 60 °C. Once a constant weight is achieved, the mass of each component is measured to calculate their respective percentages in the sample. This comprehensive analytical procedure enables the detailed quantification of different petroleum constituents within rock extracts, providing valuable insights into the hydrocarbon composition of geological samples.

Results

Minerals compositions and reservoir quality

As illustrated in Fig. 2, XRD analysis of 23 tight sandstone samples from the Chang 8 Member unveils a diverse mineral composition. Quartz is identified as the dominant mineral, with proportions ranging from 26.1 to 73.0%, and an average abundance of 49.9%. Within the analyzed samples, feldspar primarily consists of potash feldspar and plagioclase, averaging 11.33% and 21.96%,

respectively. Clay minerals, serving as the key interstitial material in these tight sandstone samples, exhibit variability from 4.6 to 23.4%, with an average presence of 12.1%. The carbonate minerals demonstrate a range from 0.3 to 10.3%, with an average of 3.6%. Among these, ferrocalcite and ankerite stand out as particularly significant, with average concentrations of 2.3% and 1.0%, respectively.

The porosity of the samples demonstrates a considerable range from 6.03 to 12.58%, with an average of 9.39%, while the permeability varies between 0.025 mD and 2.850 mD, averaging at 0.552 mD before the extraction process. After extraction, the porosity of the samples expands to a range of 7.16 to 16.82%, with an average of 12.02%. In terms of permeability, values post-extraction range from a minimum of 0.038 mD to a maximum of 3.380 mD, with an average of 0.749 mD, as depicted in Fig. 2b.

Pore types and pore sizes

The pore architectures within the tight sandstone reservoirs of the Chang 8 Member in the Ordos Basin are categorized into four distinct types: (1) residual intergranular pores (Fig. 3a–c), representing the primary pore type, are mainly observed between quartz–quartz and quartz–feldspar particle interactions, exhibiting irregular distributions and sizes ranging from 19.53 to 451.86 μm with an average of 146.69 μm ; (2) secondary dissolved pores (Fig. 3d–g), including debris dissolution and feldspar dissolution pores, with the latter often found along joint surfaces or feldspar particle edges, displaying sizes between 17.51 and 60.80 μm and an average of 34.96 μm ; (3) micropores (Fig. 3a–e), dispersed throughout, with sizes ranging from 8.08 to 23.53 μm ; and (4) inter-crystalline pores (Fig. 3h–i), detailed further in the study. The residual intergranular pores are highlighted as the most substantial within the tight sandstone framework, characterized under TS and FE-SEM as micron-scaled and irregular.

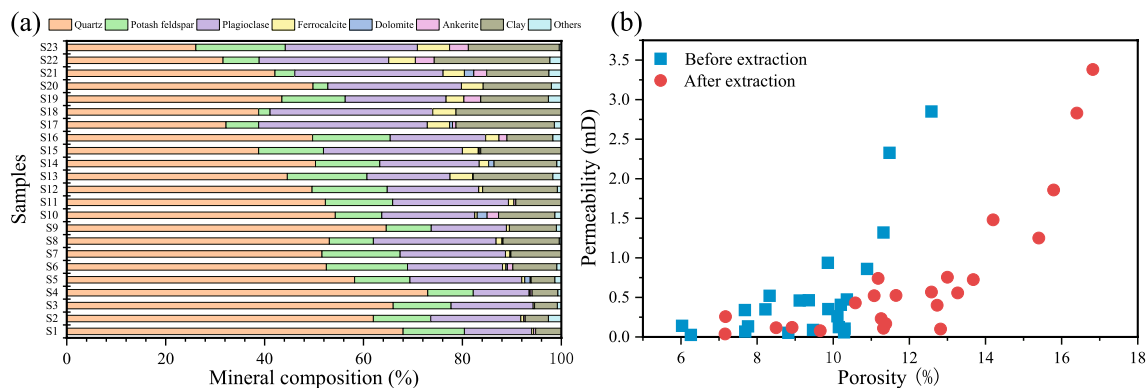
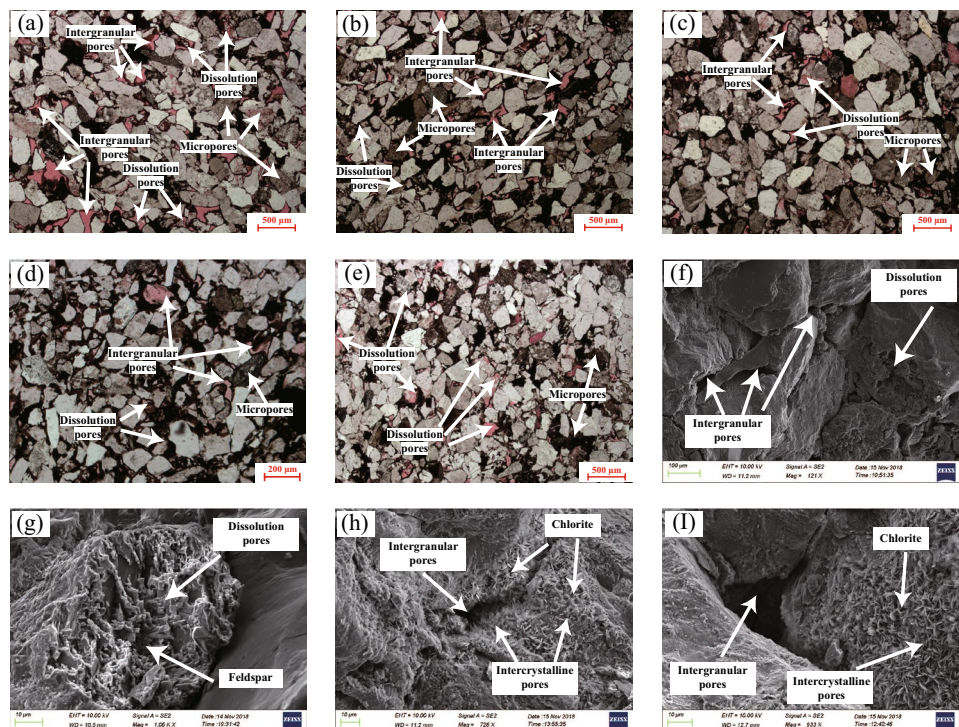


Fig. 2 a Whole rock mineral composition, and b Crossplot of porosity and permeability before and after extraction for the experimental samples

Fig. 3 Thin section and FE-SEM imagery of pore types



Feldspar dissolution pores, noted for their alignment along joint surfaces or around feldspar edges, and debris dissolution pores, filled with black clay minerals or asphalt under TS, underscore the diversity of pore types contributing to the reservoir's porosity. Micropores, with their specific size distribution, further complexify the pore structure landscape of the Chang 8 Member sandstones.

The pore structure within the Chang 8 Member tight sandstone samples, collected at various depths, showcases a diverse array of pore types, as summarized as follows: (a) Sample S1 (2148.55 m): Predominantly features residual intergranular and dissolution pores, with a minor presence of micropores. (b) Sample S2 (2138.10 m): Similar to S1, it consists mainly of residual intergranular and dissolution pores, complemented by minor micropores. (c) Sample S8 (2188.00 m): It is characterized by dissolution pores, with sparse occurrences of residual intergranular and micropores. (d) Sample S12 (2228.33 m): It also exhibits dissolution pores as the primary feature, with sparse residual intergranular and micropores. (e) Sample S23 (2144.35 m): It is dominated by dissolution pores, with minor micropores, indicating a variation in pore distribution. (f) Sample S5 (2191.30 m): It showcases a combination of residual intergranular and dissolution pores, indicating a complex pore network. (g) Sample S6 (2193.21 m): Features residual intergranular pores and an intercrystalline pore, highlighting the structural diversity within the samples. (h) Sample S12 (2228.33 m): (Repeated Sample ID with a different description) It contains residual intergranular pores and an intercrystalline

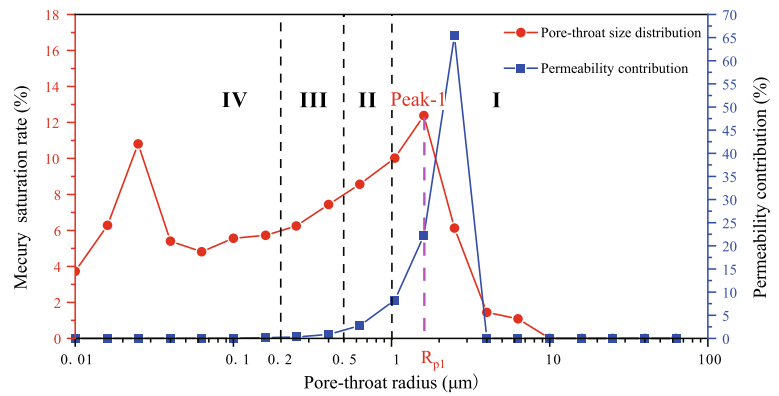
pore, underscoring the variability in pore types even within similar depth ranges. (i) Sample S16 (2288.55 m): It is characterized by secondary dissolution pores on feldspar, showcasing the chemical alteration processes affecting the reservoir rocks.

Pore structure

Pore-throat size and distribution

Leveraging the delineation criteria for HPMI curve characteristics and the first peak (Rp1) associated with tight sandstone reservoirs as outlined by Liu et al. (2021), this study classifies the pore throat architecture into four distinct categories (Fig. 4). In Type I, Rp1 surpasses 1 μm , denoting the presence of larger pore throats. Type II is characterized by Rp1 values ranging from 0.5 to 1 μm . For Type III, Rp1 falls between 0.2 and 0.5 μm , while Type IV is defined by Rp1 values less than 0.2 μm . This classification highlights the critical role larger pore throats play in enhancing the permeability of tight sandstone reservoirs (Xi et al. 2019; Liu et al. 2021). Figure 5 further illustrates the distribution of pore throat sizes and their impact on permeability across different pore structures within the tight sandstone. It is observed that Types I and II feature a wider distribution of pore throat sizes, exhibiting bimodal characteristics, whereas Types III and IV present a unimodal distribution, emphasizing the diversity in pore throat geometries and their implications for fluid flow within tight sandstone reservoirs.

Fig. 4 Differentiation of pore-throat size distribution patterns based on the radius of the first peak (R_{p1})



In this study, the R_{p1} value for Type I pore structures is identified as 2.5 μm , with the corresponding pore throat permeability contribution curve revealing a significant increase in permeability contribution rate only when the pore throat size exceeds 1 μm . For Type II, the R_{p1} value is set at 1 μm , and its permeability contribution curve shows a marked elevation in permeability contribution rate once the pore throat size surpasses 0.2 μm . In contrast, the R_{p1} values for Type III and Type IV are determined to be 0.25 μm and 0.063 μm , respectively. The pore throat permeability contribution curves for these types indicate that a substantial increase in permeability contribution rate is observed only when the pore throat size exceeds 0.4 μm for Type III and 0.02 μm for Type IV.

This detailed analysis underscores the nuanced relationship between pore throat size and its impact on the permeability of tight sandstone reservoirs. Larger pore throats, as seen in Types I and II, significantly contribute to higher permeability rates, while Types III and IV, with smaller pore throats, demonstrate a more gradual contribution to the overall permeability, highlighting the complexity of fluid flow dynamics within these reservoirs.

Pore structure parameter

Table 2 presents a comprehensive overview of the pore structure parameters for samples from the Chang 8 Member, categorized by distinct pore structure types. The tight sandstone within the Chang 8 Member displays significant heterogeneity, with notable variations in pore structure parameters observed across the range of sandstone samples. This heterogeneity becomes more pronounced with the deterioration of pore structure types, manifesting as a gradual increase in heterogeneity among the samples. Alongside this, there is a noticeable decrease in pore throat radius and a decline in throat sorting quality.

This variation underscores the complexity and diversity of pore structures within the Chang 8 Member tight sandstone, highlighting the intricate relationships between pore

structure type and reservoir properties such as porosity and permeability. Such detailed characterization is crucial for understanding fluid flow dynamics and enhancing hydrocarbon recovery strategies in these heterogeneous reservoirs.

Rock I is distinguished by its low displacement pressure, expansive pore throats, notable homogeneity, and excellent throat sorting. Maximum mercury saturation is observed within a range of 83.10–86.83%, with mercury removal efficiency between 29.23% and 33.44%. Displacement pressures vary from 0.03 to 0.08 MPa, while capillary median pressures span from 1.80 to 5.18 MPa. Additionally, maximum and average pore throat radii are found within ranges of 9.19 μm to 24.15 μm and 1.24 μm to 3.30 μm , respectively. Structure coefficients range from 1.28 to 1.92, with throat sorting coefficients between 2.94 and 3.27. For Type II, the parameter distribution shifts. Maximum mercury saturation ranges from 84.33 to 90.17%, and mercury removal efficiency from 23.25 to 38.28%. Displacement pressure varies between 0.20 to 0.60 MPa, with capillary median pressures extending from 1.71 to 8.46 MPa. The maximum and average pore throat radii are within ranges of 2.45–3.68 μm and 0.42–0.60 μm , respectively. Structure coefficients exhibit a broader range from 0.35 to 6.14, and throat sorting coefficients range from 2.15 to 2.80. Type III features a maximum mercury saturation range of 80.88 to 93.58% and a mercury removal efficiency range of 24.28 to 34.29%. Displacement pressures are distributed from 0.30 to 1.79 MPa, with capillary median pressures ranging from 2.58 to 10.83 MPa. Maximum and average pore throat radii vary between 1.47 to 2.81 μm and 0.17 to 0.45 μm , respectively. The structure coefficient ranges from 0.26 to 3.44, with throat sorting coefficients observed within 1.79 to 2.36. Type IV exhibits high displacement pressure, smaller pore throats, marked heterogeneity, and poor throat sorting. Maximum mercury saturation spans from 79.57 to 93.37%, with mercury removal efficiency between 28.49% and 40.19%. Displacement pressure ranges from 0.80 to 3.72 MPa, while capillary median pressures are between 7.89 to 22.40 MPa. The maximum and average pore throat radii are within ranges of

Table 2 Pore structure parameters of tight sandstone reservoirs as determined by HPMI

Samples	Depth (m)	Maximum injection saturation (%)	With-drawal efficiency (%)	D_p (MPa)	C_p (MPa)	R_{max} (μm)	R_{Ave} (μm)	Structural coefficient (a.u.)	Throat sorting coefficient (a.u.)
S1	2148.6	86.83	29.23	0.03	1.80	24.51	2.51	1.92	3.09
S2	2138.1	86.41	33.13	0.08	4.12	9.19	1.24	1.28	2.94
S3	2147.9	84.38	29.63	0.03	1.95	24.51	3.30	1.64	3.27
S4	2149.5	83.10	33.44	0.05	5.18	14.71	1.56	1.74	3.13
S5	2191.3	84.33	37.42	0.20	7.14	3.68	0.55	0.35	2.80
S6	2193.2	85.10	33.72	0.30	4.90	2.45	0.42	0.38	2.65
S7	2242.4	86.92	23.25	0.20	1.71	3.68	0.60	1.12	2.39
S8	2188.0	87.06	38.28	0.30	8.46	2.45	0.46	0.66	2.62
S9	2287.5	90.17	26.55	0.57	2.03	3.60	0.47	4.07	2.50
S10	2134.2	89.28	33.44	0.60	2.11	2.82	0.45	6.14	2.15
S11	2062.2	91.91	33.18	0.30	3.17	2.45	0.45	0.51	2.36
S12	2228.3	88.15	28.69	1.01	10.83	2.81	0.17	0.73	2.09
S13	2239.7	91.67	28.55	0.50	2.58	1.47	0.31	0.36	2.19
S14	2192.6	93.25	33.66	0.30	3.72	2.45	0.41	0.43	2.32
S15	2168.5	84.60	24.28	0.50	3.63	1.47	0.27	0.82	2.36
S16	2288.6	91.16	33.78	0.50	5.37	1.47	0.31	0.38	2.30
S17	2235.6	80.88	34.29	1.79	4.62	2.79	0.18	3.44	1.79
S18	1956.3	93.58	30.17	0.50	7.47	1.47	0.19	0.26	1.94
S19	2296.2	88.20	34.96	3.72	20.70	1.85	0.07	0.81	1.55
S20	2238.2	87.16	28.49	2.00	7.89	0.37	0.11	0.10	2.08
S21	2163.8	97.37	31.58	0.80	13.16	0.92	0.09	0.07	1.44
S22	2546.3	90.59	40.19	1.50	12.51	0.49	0.09	0.07	1.92
S23	2144.4	79.52	37.85	2.09	22.40	1.87	0.09	1.21	1.74

D_p displacement pressure; C_p capillary median pressure; R_{max} maximum pore throat radius; R_{Ave} average throat radius

0.37–1.87 μm s and 0.07 to 0.11 μm , respectively. Structure coefficients are distributed from 0.07 to 1.21, with throat sorting coefficients varying between 1.44 and 2.08. Above detailed summary delineates the pore structure parameters for the Chang 8 Member tight sandstone samples, highlighting the distinct characteristics of each pore structure type and their implications for reservoir quality and hydrocarbon extraction efficiency.

Reservoir types

In this study, the classification of reservoir types within the Chang 8 tight sandstone reservoirs is conducted based on a comprehensive analysis that includes lithology, pore types, pore structure categories, and pore size distribution characteristics. This classification is systematically illustrated in Fig. 5, providing a detailed visual representation of the various reservoir types identified within the Chang 8 Member. This approach allows for a nuanced understanding of the reservoir's heterogeneity, encompassing the diversity of rock compositions, the assortment of pore types ranging from intergranular to micropores, and the variation in pore

structure categories that define the reservoir's porosity and permeability profiles. Additionally, the pore size distribution characteristics offer insights into the fluid flow dynamics and potential hydrocarbon recovery strategies pertinent to each reservoir type. This multi-faceted classification scheme serves as a foundational aspect of evaluating the Chang 8 tight sandstone reservoirs, facilitating targeted exploration and development efforts within the Ordos Basin.

This study meticulously delineates the characteristics of four distinct reservoir rocks within the Chang 8 tight sandstone reservoirs, highlighting their lithological composition, porosity and permeability metrics, predominant pore types, and pore structure categorizations: Rock I exhibits medium porosity and low permeability, with values ranging from 15.40 to 16.82% (average 16.10%) and 1.250 to 3.380 mD (average 2.329 mD), respectively. This reservoir, primarily composed of lithic arkose, features residual intergranular and feldspar dissolved pores, with debris dissolved pores as a secondary pore type. Classified as Type I, its pore-throat size distribution shows a bimodal characteristic, significantly spanning from 0.01 to 30 μm , where the R_{p1} value exceeds 1 μm . Rock II, characterized by feldspar litharenite lithology,

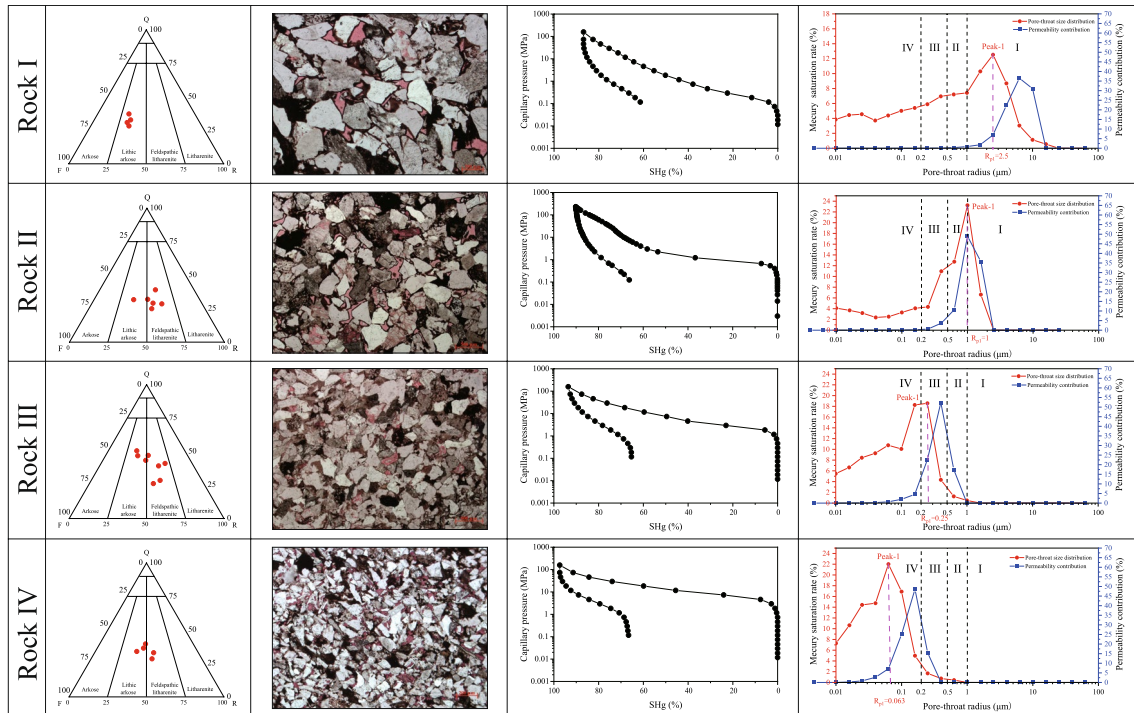


Fig. 5 Classification scheme of Chang 8 tight sandstone reservoirs

displays low porosity and low permeability, with porosity values between 11.65% and 14.20% (average 13.06%) and permeability ranging from 0.524 to 1.480 mD (average 0.768 mD). The reservoir's pore structure is identified as Type II, primarily consisting of residual intergranular and feldspar dissolved pores, alongside micropores. Its pore-throat size distribution extends from 0.01 to 3 μm , showing a single peak characteristic, with R_{p1} values ranging from 0.5 to 1 μm . Rock III reveals low porosity and low permeability, with porosity spanning 10.58 to 12.82% (average 11.54%) and permeability from 0.100 to 0.740 mD (average 0.337 mD). Comprising feldspar litharenite and lithic arkose, it is marked by the presence of residual intergranular, feldspar dissolved, and intercrystalline pores, fitting into the Type III pore structure category. The pore-throat size distribution broadly ranges from 0.01 to 1 μm , exhibiting a single peak characteristic, where R_{p1} values are observed between 0.2 and 0.5 μm . Rock IV is distinguished by its ultra-low porosity and permeability, with porosity values ranging from 7.16 to 9.66% (average 8.28%) and permeability between 0.038 and 0.257 mD (average 0.122 mD). Its lithology, predominantly feldspar litharenite and lithic arkose, features feldspar dissolved and intercrystalline pores, categorized under Type IV pore structure. The pore-throat size distribution extends from 0.01 to 0.5 μm , showing a single peak characteristic, with an R_{p1} value noted to be less than 0.2 μm . This comprehensive analysis provides a clear insight into the variability and complexity of pore structures within the Chang 8

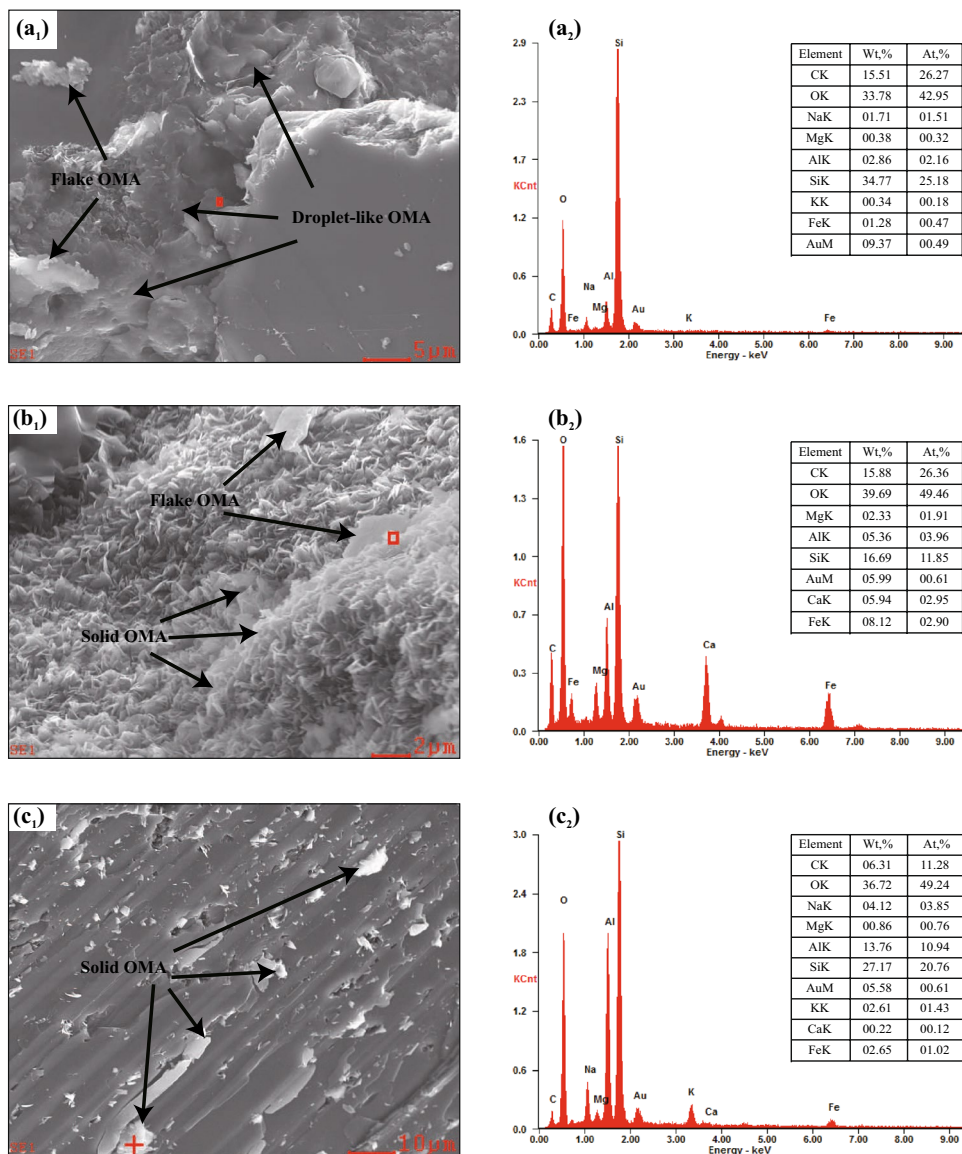
Member tight sandstone reservoirs, underlining the intricate interplay between lithology, pore characteristics, and reservoir properties.

Micro-occurrence states of residual oil

Location and morphology

The distribution of crude oil within the reservoir space of the Chang 8 Member tight sandstone is significantly influenced by interactions between oil–rock and oil–oil, predominantly manifesting as oil–mineral aggregates (OMA) on the surfaces of pores and mineral particles. This phenomenon underscores the complex nature of hydrocarbon storage mechanisms in tight sandstone reservoirs (Li et al. 2018a; Bai et al. 2019; Taheri-Shakib et al. 2019a, b; Zhou et al. 2022b). ESEM analysis of the residual oil morphology within these reservoirs reveals three distinct micro-occurrence states of residual oil: droplet-like OMA, flake OMA, and solid OMA, as depicted in Fig. 6. These forms of residual oil, each with unique structural characteristics, illustrate the varied ways in which oil is retained and distributed within the pore spaces of tight sandstone formations. Furthermore, the presence of residual oil across various pore types highlights the heterogeneity of the reservoir matrix and the intricate interplay between geological textures and hydrocarbon accumulation processes. This detailed understanding of oil micro-occurrence states offers

Fig. 6 Microscopic manifestations of residual oil under ESEM



valuable insights into the efficiency of hydrocarbon recovery and the potential challenges faced during extraction from tight sandstone reservoirs.

Within the Chang 8 Member tight sandstone reservoirs, the residual intergranular pores emerge as the primary sites for the accumulation of residual oil. This residual oil is predominantly found in the form of droplet-like OMA, with a lesser quantity of flake OMA also present along the edges of these pores, as shown in Fig. 6a₁. Such accumulations occupy a significant portion of the reservoir space, underscoring the importance of residual intergranular pores in storing residual oil. EDS tests identify a carbon content of 15.51% within the residual

oil in these pores (Fig. 6a₂), highlighting their considerable oiliness. In contrast, within the intercrystalline pores coated with chlorite, residual oil is primarily found in solid OMA form. On the surfaces of chlorite particles, residual oil more commonly appears in flake OMA form (Fig. 6b₁). EDS analysis of these intercrystalline pores reveals a carbon content of 15.88% (Fig. 6b₂), indicating a high level of oiliness, similar to that observed in the intergranular pores. For feldspar dissolution pores, the residual oil mainly assumes a solid OMA form (Fig. 6c₁), with a lesser portion appearing as a bright white ring edge around the boundaries of these pores, suggesting a distinct mode of occurrence. EDS results for the oil

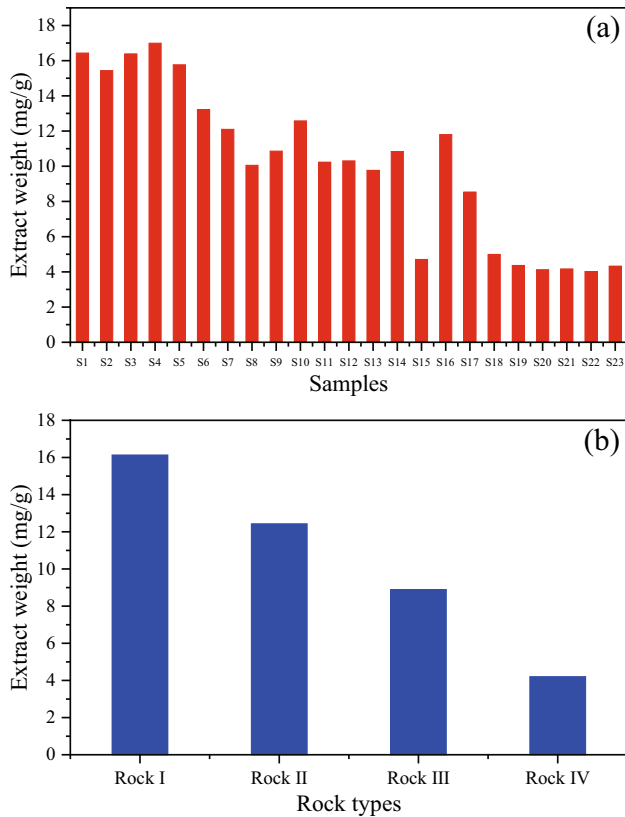


Fig. 7 Variation in extract weight of residual oil (a) and its association with reservoir types (b) in Chang 8 Member tight sandstones

within feldspar dissolution pores show a carbon content of 6.31% (Fig. 6c₂), pointing to relatively lower oiliness compared to the other pore types. This analysis provides a detailed insight into the different states and distributions of residual oil within the Chang 8 Member, illustrating the variability in oiliness and the role of pore type in influencing the accumulation and preservation of hydrocarbons in tight sandstone reservoirs.

Extract weight

The presence of residual oil as immobile oil within the tight sandstone reservoir spaces is a significant factor, especially considering the low recovery factor (below 10%) associated with existing extraction methods for such reservoirs (Liu et al. 2021). This underscores the importance of quantifying the amount of crude oil present as residual oil to potentially enhance future oil recovery efforts. Analysis of extraction results from the Chang 8 tight sandstone of the Ordos Basin (Fig. 7) indicates a substantial quantity of residual oil, with extract weights ranging from 4.02 to 16.99 mg/g and an average of 10.08 mg/g (Fig. 7a). Yet, there are significant variations in residual oil content across different reservoir types (Fig. 7b): Rock I shows a high concentration of residual oil,

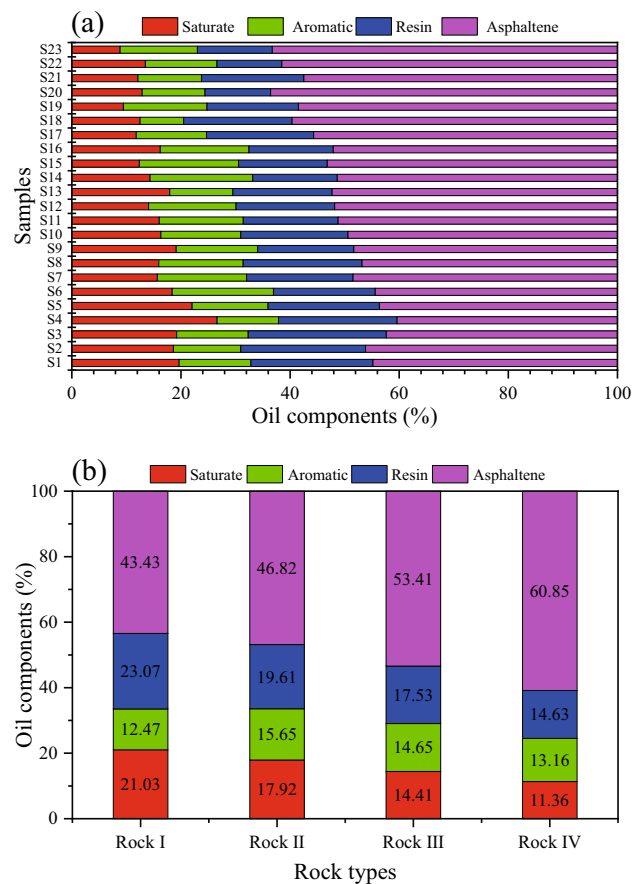


Fig. 8 Composition of residual oil (a) and its variation across reservoir types (b) in Chang 8 Member tight sandstones

with extract weights ranging from 15.43 to 16.99 mg/g, and an average of 16.31 mg/g. This suggests that Rock I has the highest potential for oil recovery among the analyzed reservoir types. Rock II has a moderate level of residual oil, with extract weights between 10.05 mg/g and 15.76 mg/g, and an average of 12.43 mg/g. This indicates a significant but lesser amount of residual oil compared to Rock I. Rock III's extract weight varies from 4.70 to 11.80 mg/g, with an average of 8.89 mg/g, pointing to a lower concentration of residual oil, which may impact recovery strategies. Rock IV exhibits the lowest concentration of residual oil among the types, with extract weights ranging from 4.02 to 4.37 mg/g and an average of 4.20 mg/g. This indicates a substantial decrease in the potential for oil recovery in this reservoir type.

The distribution of residual oil in these tight sandstone reservoirs diminishes in line with the deterioration of reservoir types, revealing a clear relationship between reservoir characteristics and the quantity of immobile oil. Understanding these distributions is crucial for developing targeted and effective enhanced oil recovery (EOR) strategies tailored to the specific properties of each reservoir type within the Ordos Basin.

Oil components

Crude oil's composition, encompassing saturates, aromatics, resins, and asphaltenes (SARA), plays a crucial role in defining the micro-occurrence states of residual oil within tight sandstone reservoirs, as these components differentially accumulate due to interactions with the pore-throat media (Li et al. 2018a). An in-depth analysis of the residual oil's compositional makeup is pivotal for devising more effective extraction strategies in the petroleum industry. The compositional analysis of the Chang 8 tight sandstone reservoir's residual oil (Fig. 8) demonstrates that the residual oil within the Chang 8 tight sandstone reservoir is significantly dominated by the heavier components, resins, and asphaltenes, which together account for an average of 69.98% of the oil. In contrast, the lighter components, saturates and aromatics, collectively constitute a lower average of 30.02%. This predominance of heavier components suggests that the extraction and recovery processes face challenges due to the higher viscosity and lower mobility associated with such compositions. Understanding these compositional nuances is vital for tailoring extraction methods that can efficiently mobilize and recover the diverse components of residual oil from tight sandstone reservoirs.

The compositional analysis of oil components within the Chang 8 tight sandstone reservoirs reveals significant variations across different reservoir types, as detailed in Fig. 8b. The distribution of SARA components across these reservoir types highlights the influence of reservoir quality on the composition of residual oil: Rock I has average SARA contents of 21.03% S, 12.47% A, 23.07% R, and 43.44% A. This reservoir type, characterized by relatively better reservoir quality, shows a balanced distribution of SARA components with a lower asphaltene content compared to other types. Rock II's average contents are 17.92% S, 15.65% A, 19.61% R, and 46.82% A. The increase in asphaltene content and a slight reduction in saturate and resin contents reflect a shift toward heavier components as reservoir quality begins to decline. Rock III presents average concentrations of 14.41% S, 14.65% A, 17.53% R, and 53.41% A. The notable rise in asphaltene content and further reduction in the lighter components indicate significant changes in oil composition correlating with further deterioration in reservoir quality. Rock IV shows average contents of 11.36% S, 13.16% A, 14.63% R, and 60.85% A. This type, representing the poorest reservoir quality, has the highest asphaltene content, indicating the most significant shift toward heavier and more complex molecular structures in the residual oil.

As the reservoir quality declines from Rock I to Rock IV, a clear increase in asphaltene content within the residual oil extracts is observed, with a corresponding reduction in the contents of saturates, aromatics, and resins. Notably, the saturate content experiences a reduction by approximately

46%, underscoring the shifts in residual oil composition. This trend highlights the elevated asphaltene content associated with the deterioration of reservoir types, suggesting that reservoir quality significantly influences the chemical makeup of residual oil. Understanding these compositional shifts is crucial for developing targeted and effective extraction strategies that can address the challenges posed by the varying oil compositions across different reservoir types.

Discussion

Porosity and permeability reduction effect of residual oil and its influencing factors

Porosity and permeability reduction effect of residual oil

The presence of residual oil within porous media significantly influences the physical properties of reservoir rocks, particularly impacting porosity and permeability. These changes have crucial consequences for the migration and extraction of oil and gas, especially in tight sandstone reservoirs (Bolouri and Ghoojani 2012; Hematfar et al. 2018; Taheri-Shakib et al. 2018, 2019a). A detailed examination of the Chang 8 tight sandstone reservoir's porosity and permeability, conducted before and after extraction experiments (Table 1), demonstrates that residual oil significantly hinders the reservoirs' porosity and permeability. Specifically, porosity decreases by a range of 0.81% to 4.92%, with an average reduction of 2.63%, while permeability decreases by 0.013 mD to 0.543 mD. Following the extraction, an increase in reservoir porosity is observed, ranging from 9.32 to 44.02%, with an average increase of 27.19%. Simultaneously, permeability exhibits an average enhancement of 46.49%.

These observations indicate that the adverse effects of residual oil enrichment on reservoir permeability are markedly more significant than on porosity. This disparity is likely due to the small throat sizes characteristic of tight sandstone reservoirs. When crude oil accumulates on the throat surfaces, it can further narrow or even completely block the original throat dimensions, severely restricting fluid flow. This accumulation not only reduces the effective pore space available for hydrocarbon storage but also significantly diminishes the reservoir's ability to transmit fluids, thereby impacting recovery processes. Addressing the challenges posed by residual oil in such reservoirs is essential for enhancing oil and gas recovery strategies, highlighting the importance of understanding and mitigating its effects on reservoir properties.

Figure 9 showcases the negative impact of residual oil on the pore throat dimensions of tight sandstone reservoirs, highlighting improvements in porosity and permeability across various reservoir types post-extraction. The observed

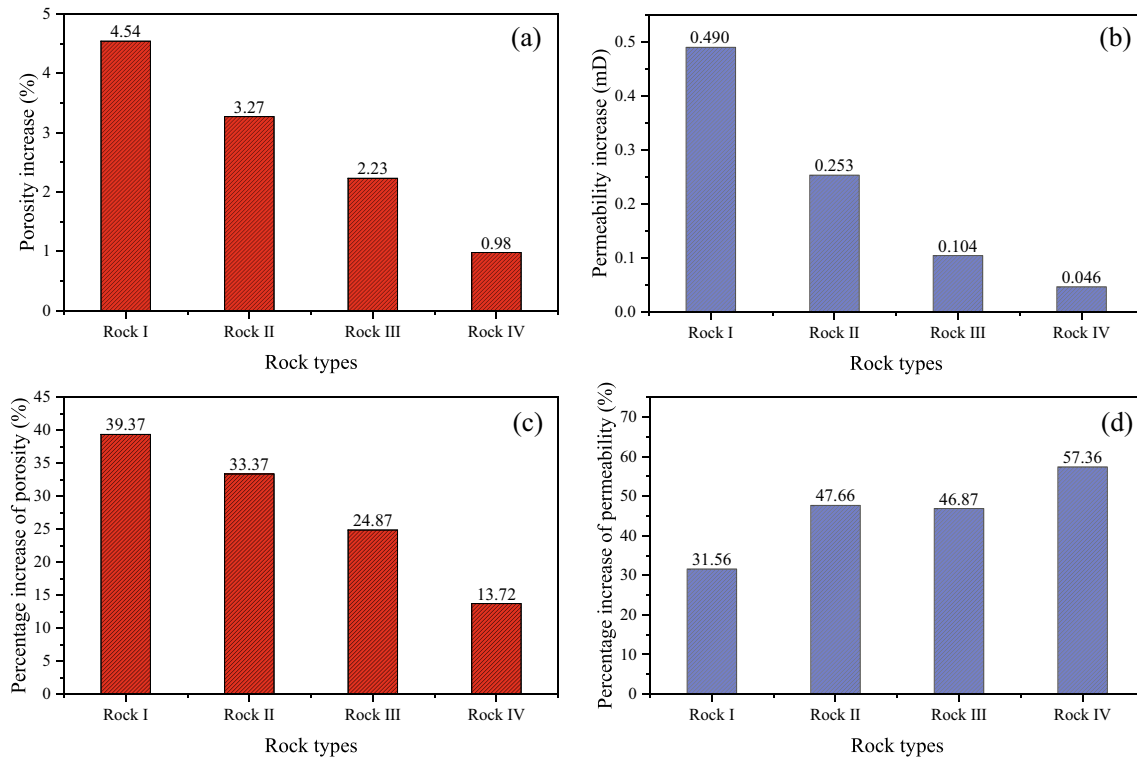


Fig. 9 Impact of residual oil distribution on reduction of reservoir porosity and permeability. **a** porosity reduction; **b** permeability reduction; **c** proportion of porosity reduction; **d** proportion of permeability reduction

increments in porosity for these reservoir types are 4.54%, 3.27%, 2.23%, and 0.98%, respectively (Fig. 9a). Likewise, enhancements in permeability are recorded as 0.490 mD, 0.253 mD, 0.104 mD, and 0.046 mD, respectively (Fig. 9b), revealing a declining trend in both porosity and permeability increments as reservoir quality deteriorates.

The basis for these findings lies in the initial porosity of the reservoirs; higher initial porosity provides more space for crude oil accumulation within the reservoir. Moreover, superior permeability enables easier migration of crude oil into the reservoir spaces during the filling process, thereby facilitating oil and gas enrichment. This environment also allows for extensive interactions between a significant volume of crude oil and the reservoir's porous medium. Within these dynamics, especially the heavy components of crude oil are likely to be adsorbed due to their interaction with the pore throat medium, leading to heavy component accumulation.

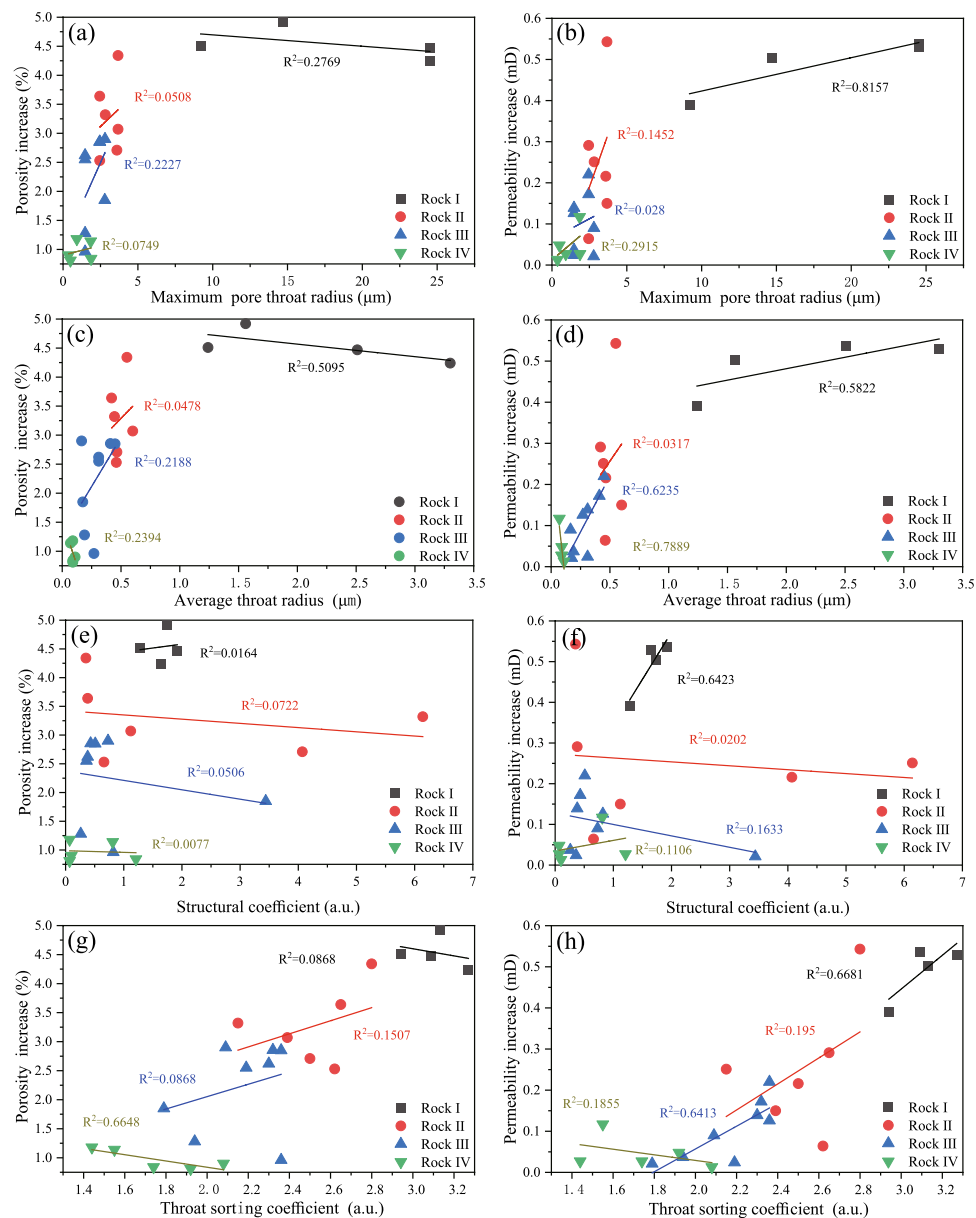
The percentage increase in porosity across the different reservoir types is noted as 39.37%, 33.37%, 24.87%, and 13.72%, respectively, showing a downward trend with the deterioration of reservoir quality (Fig. 9c). Conversely, the trend in the percentage increase in permeability is inverse relative to that of porosity, with the percentage increase in permeability rising as the reservoir quality worsens (Fig. 9d). This pattern highlights the significant role of residual oil enrichment within the reservoir, particularly

in suboptimal reservoir types, where its adverse effects on pore throat dimensions become increasingly evident. These insights emphasize the need for targeted strategies to mitigate the impact of residual oil, especially in lower-quality reservoirs, to enhance oil recovery efforts.

Effects of pore structure on porosity and permeability reduction

Figure 10 provides insight into how different reservoir types within the Chang 8 Member tight sandstone respond variably to the impact of residual oil on pore throat dimensions. The analysis reveals that the relationship between changes in reservoir properties (porosity and permeability) and the maximum pore throat radius differs across reservoir types: In Rock I, II, and III, there exists a weak positive correlation between the increments in reservoir porosity and the maximum pore throat radius, indicating that as the size of the largest pore throats increases, there is a slight corresponding increase in porosity. However, in Rock IV, this relationship turns mildly negative (Fig. 10a), suggesting that an increase in the maximum pore throat radius may slightly decrease porosity, reflecting the unique response of Rock IV's pore structure to residual oil effects. A slight positive correlation is observed between the reservoir permeability increment and the maximum pore throat radius in Rock I, II,

Fig. 10 Influence of pore structure parameters on porosity and permeability reduction across different reservoir types



and III, contrasting sharply with Rock IV, which exhibits a significant positive correlation, underscored by a correlation coefficient of 0.8157 (Fig. 10b). This indicates that Rock IV's permeability is more sensitively tied to changes in the maximum pore throat radius compared to the other types. The relationship between the average pore throat radius and the porosity increment is weakly negative in Rock I and IV, but faintly positive in Rock II and III (Fig. 10c). This suggests varying degrees of influence that the average size of pore throats has on the overall porosity increment across different reservoir types. Moreover, a notable negative correlation between the average pore throat radius and the permeability increment is observed in Rock I, whereas Rock II, III, and IV show a positive correlation (Fig. 10d). This divergence highlights the complex interaction between pore throat

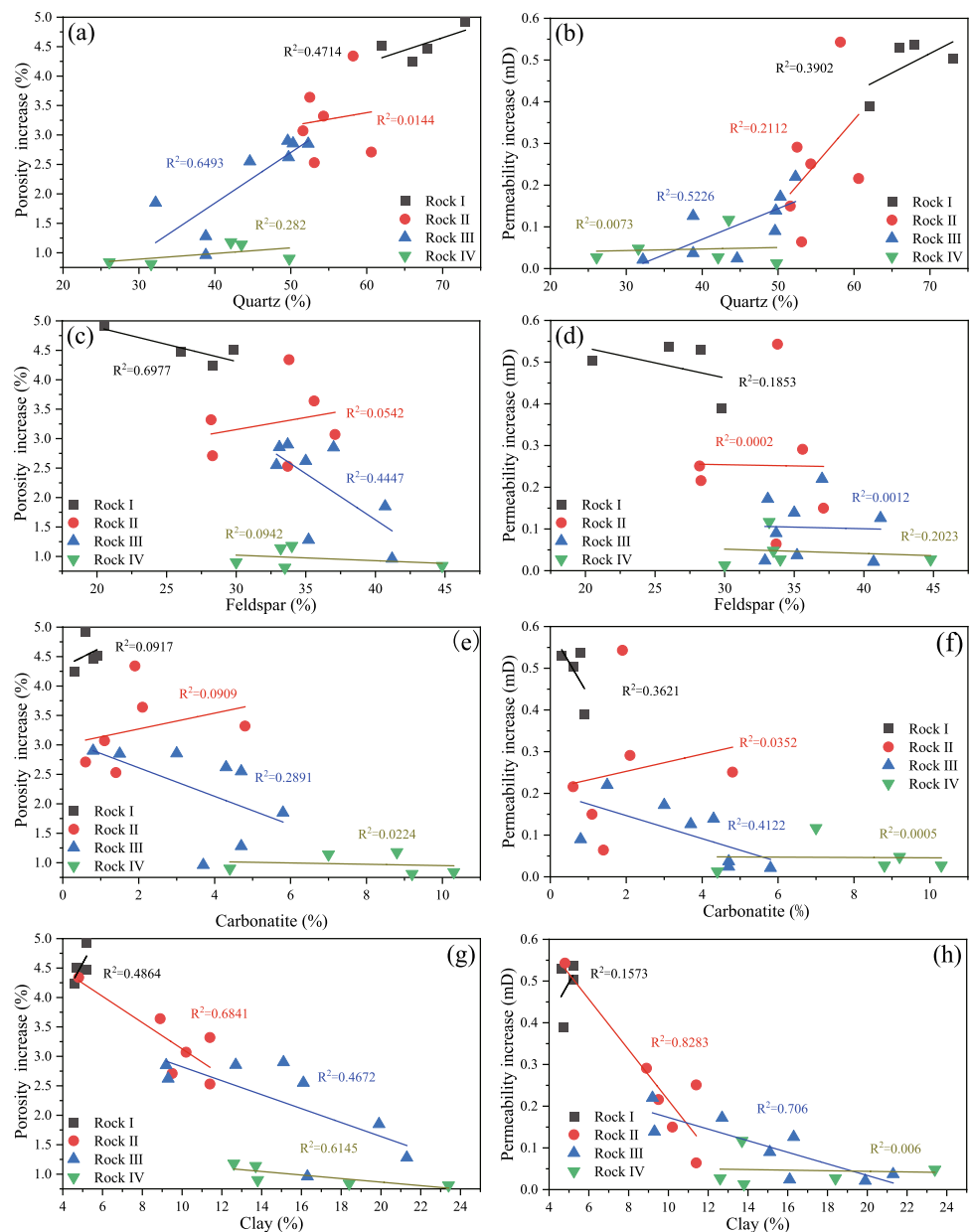
dimensions and permeability enhancements post-extraction, with Rock I showing a distinct pattern from the others. These correlations imply that while larger original pore throats in the reservoir generally facilitate residual oil enrichment, the specific response to reducing residual oil varies among different reservoir types, likely due to the pronounced heterogeneity characteristic of tight sandstone reservoirs.

Figure 10 demonstrates the complex relationships between reservoir structural and throat sorting coefficients and the variations in porosity and permeability across different reservoir types within the Chang 8 Member tight sandstone. The analysis reveals that: There is no discernible correlation between the reservoir's structural coefficient and the increments of porosity and permeability across Rock II, Rock III, and Rock IV (Fig. 10e, f). This lack of correlation

suggests that the distribution and impact of residual oil on these reservoir characteristics might be influenced by factors beyond just the structural coefficient, such as pore throat geometry and connectivity. However, Rock I presents an exception where a positive correlation exists between the reservoir's structural coefficient and the increments of both porosity and permeability, with a notably stronger correlation with the permeability increment. This pattern indicates that in Rock I, characterized by relatively well-sorted pores and minor variance in pore sizes, the structural coefficient plays a significant role in influencing porosity and permeability. The substantial amount of residual oil in Rock I, facilitated by its pore structure, likely contributes to this correlation. Conversely, the throat sorting coefficient shows

a positive correlation with the increments of porosity and permeability across most reservoir types, except for a negative correlation in Rock IV (Fig. 10g, h). This suggests that better throat sorting generally makes the reservoir's porosity and permeability more vulnerable to the negative impacts of residual oil, potentially due to the facilitation of crude oil seepage within the reservoir. The observed negative correlation in Rock IV might indicate that in cases of poor throat sorting, the effects of residual oil on porosity and permeability become less predictable, possibly due to more heterogeneous pore throat distributions that complicate the migration and entrapment of oil. These findings highlight the nuanced interplay between pore structure characteristics and the behavior of residual oil within tight sandstone

Fig. 11 Impact of mineral compositions on porosity and permeability reduction across different reservoir types



reservoirs. The variability in correlations across different reservoir types underscores the heterogeneity inherent in these reservoirs and the need for tailored recovery strategies that consider the specific structural and sorting characteristics of each reservoir type. Understanding these dynamics is crucial for optimizing oil recovery, particularly in tight sandstone formations where traditional extraction methods are less effective.

Effects of mineral composition on porosity and permeability reduction

The study's exploration into the relationship between mineral composition discrepancies and changes in porosity and permeability (Fig. 11) illuminates the intricate dynamics between minerals and crude oil interactions within tight sandstone reservoirs. Key findings from this analysis reveal that: (1) Quartz Content: As the primary framework mineral, quartz significantly impacts the compressive strength of tight sandstone reservoirs. A positive correlation between quartz content and increments in porosity and permeability is observed (Fig. 11a, b). This suggests that higher quartz content, indicative of a well-developed mineral framework, enhances the reservoir's capacity for oil storage and fluid transmission due to its contribution to structural integrity. (2) Feldspar Content: The relationship between feldspar content and changes in porosity and permeability varies, showing no discernible correlation or even a negative correlation (Fig. 11c, d). This variability can be attributed to feldspar dissolution processes within the reservoir, which, while potentially increasing pore space, may also reduce the reservoir's resistance to compaction and increase heterogeneity. These effects can complicate fluid flow and trap residual oil, limiting the effectiveness of extraction efforts. (3) Carbonate and Clay Mineral Content: Both carbonate and clay minerals, as interstitial substances, are identified as critical factors contributing to reservoir densification. There is a general negative correlation between these mineral contents and the increments in porosity and permeability (Fig. 11e–h), suggesting that an abundance of these minerals can restrict crude oil infiltration, reduce reservoir space, and disrupt pore throat connectivity. However, a weak positive correlation is noted in Rock I and Rock II, potentially due to their lesser quantities of carbonates and clays, which translates to a less severe impact on reservoir quality.

These insights underscore the significant role mineral composition plays in defining the physical properties and fluid dynamics of tight sandstone reservoirs. The presence and interaction of different minerals with crude oil not only dictate the porosity and permeability of these reservoirs but also influence their response to extraction techniques. Understanding these mineralogical influences is paramount for developing tailored approaches to enhance oil recovery,

particularly in reservoirs where conventional methods show limited efficacy. The nuanced relationship between mineral content and reservoir characteristics highlights the necessity of integrating geologic, petrologic, and engineering perspectives to optimize recovery strategies in tight sandstone formations.

Controlling factors of residual oil distribution

Effects of porosity and permeability on the content of residual oil

The accumulation of residual oil within reservoirs significantly influences the reduction of pore and throat dimensions in tight sandstone formations, serving as a major impediment to the effective migration and extraction of hydrocarbons (Alimohammadi et al. 2019; Davudov and Moghanloo 2019; Taheri-Shakib et al. 2019a, b; Mohammed et al. 2021). This effect is largely due to the interaction between the residual oil components, particularly heavier molecules like asphaltenes, and the mineral surfaces of the reservoir rock. These interactions can lead to the adsorption of oil components onto the pore walls, effectively narrowing the

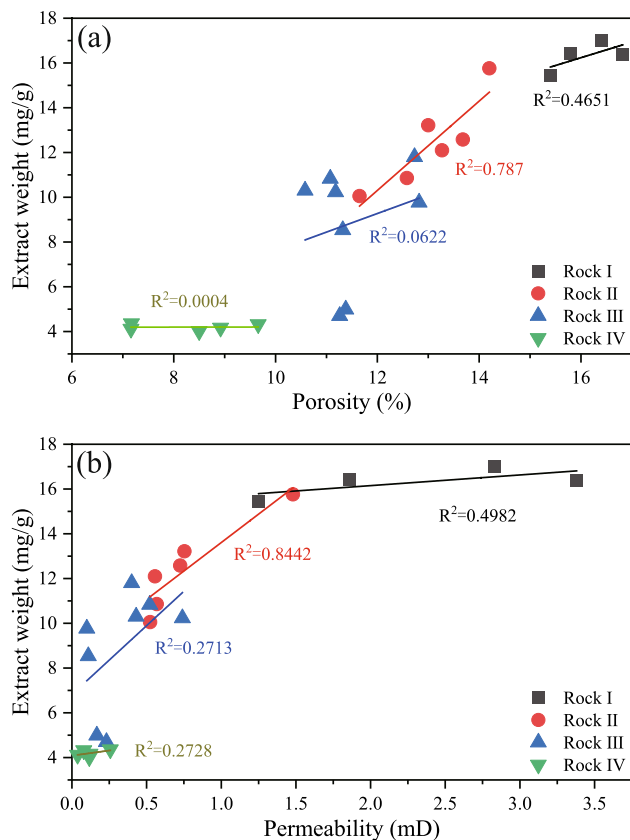


Fig. 12 Impacts of **a** Porosity and **b** Permeability on residual oil distribution across different reservoir types

pore throats and reducing the overall porosity and permeability of the formation.

The spatial dimensions of the reservoir and the connectivity of its pore throats are recognized as pivotal factors that govern the distribution and mobility of crude oil within tight sandstone reservoirs (Huang et al. 2021; Liu et al. 2021). Tight sandstone formations, characterized by their low porosity and permeability, pose unique challenges for hydrocarbon recovery due to the restricted flow paths for oil and gas. The presence of residual oil exacerbates these challenges, as it can lead to further occlusion of pore throats and diminish the effectiveness of enhanced oil recovery (EOR) techniques.

A positive correlation exists between the initial porosity and permeability of the reservoir and the effectiveness of residual tight oil extraction, as illustrated in Fig. 12. The correlation coefficient that links porosity to extraction efficiency across different reservoir types (Fig. 12a) is found to be lower than that for permeability (Fig. 12b). This suggests that reservoirs with superior initial physical properties, particularly permeability, are more favorable environments for the accumulation and subsequent extraction of residual oil. The observed ascending trend in the correlation between porosity, permeability, and extraction efficiency in Rock II, Rock III, and Rock IV highlights the crucial role of initial physical properties in determining the presence and extractability of residual oil within these reservoirs. Notably, Rock IV, characterized by relatively lower porosity and permeability, exhibits suboptimal seepage efficiency for crude oil, leading to a less pronounced correlation between its initial physical properties and the extracted residual oil content. This suggests that the efficiency of oil extraction from Rock IV may be adversely affected by its tighter physical

attributes. Furthermore, the distribution of residual oil in Rock I could be subject to additional geological factors beyond the initial physical properties of the reservoir, indicating a complex interplay of variables influencing oil occurrence and recoverability in tight sandstone formations. This nuanced understanding of the relationship between reservoir properties and oil extraction underscores the importance of considering a broad range of geological and physical factors in optimizing recovery strategies for tight oil reservoirs.

Effects of pore structure on the content of residual oil

The heterogeneity of pore structures in tight sandstone reservoirs plays a crucial role in determining the variations in crude oil percolation capabilities and its subsequent accumulation within these reservoirs (Pang et al. 2022). This variability in pore structures significantly influences the mobility of crude oil, affecting how effectively it can move through the reservoir and accumulate in various pore spaces (Zhang et al. 2022). The intricate pore networks, characterized by their varying sizes, shapes, and connectivity, dictate the flow paths available for crude oil migration (Yang et al. 2022). In reservoirs where the pore structure exhibits a high degree of heterogeneity, crude oil percolation can be uneven, leading to differential accumulation patterns. This heterogeneity not only challenges the extraction of crude oil but also emphasizes the importance of detailed reservoir characterization in predicting and enhancing recovery efforts. As such, examining the impact of pore structure disparities on the presence of residual oil becomes a key aspect of understanding the microscale processes governing the accumulation of residual oil within tight sandstone reservoirs.

Fig. 13 Impact of pore structure parameters on residual oil distribution across different reservoir types

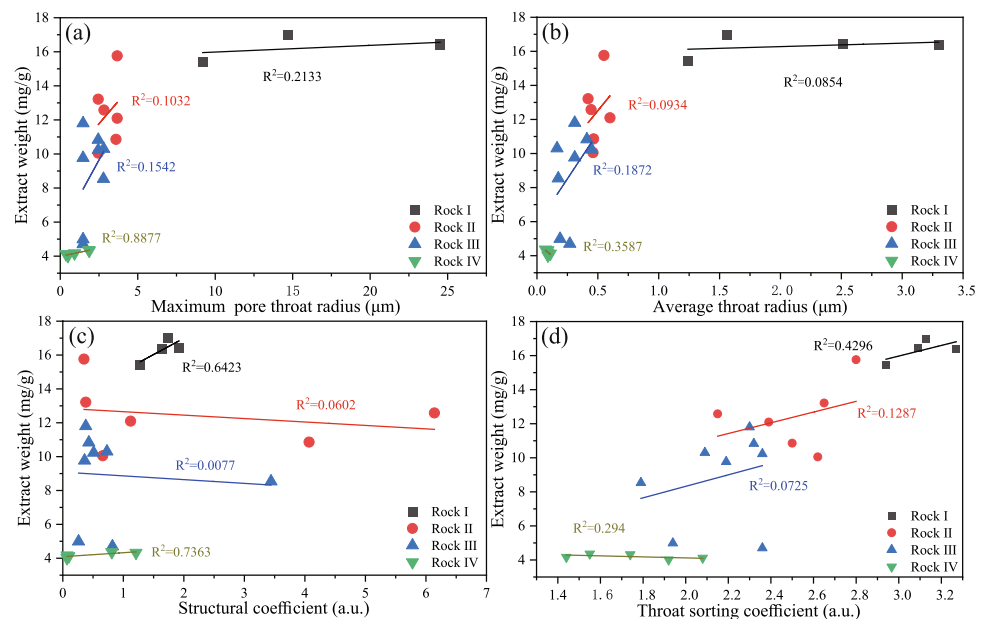


Figure 13 highlights the relationship between pore structure parameters and the extract weight of residual oil, revealing key insights into how pore characteristics influence residual oil distribution within tight sandstone reservoirs. A positive correlation is identified between both the maximum and average pore throat radii and the residual oil extract (Fig. 13a, b). This correlation suggests that larger pore throats within the reservoir serve as the primary sites for residual oil accumulation. The significant variability in pore throat distributions across different reservoirs, a manifestation of the pronounced heterogeneity inherent in these formations, results in noticeable differences in the accumulation of residual oil across varying pore spaces.

A substantial positive correlation between the structural coefficient and the extract weight of residual oil is observed in Rock I and Rock IV (Fig. 13c), with correlation coefficients of 0.6423 and 0.7363, respectively. This indicates that in these particular reservoir types, the structural framework significantly influences the capacity for residual oil enrichment. Conversely, Rock II and Rock III display a weak negative correlation, suggesting that the structural characteristics of these reservoirs may not be as conducive to oil accumulation.

Moreover, a mild positive correlation is detected between the throat sorting coefficient and the extract weight of residual oil (Fig. 13d), with the correlation becoming stronger in reservoirs with improved types. This trend highlights the role of uniformity in pore and throat dimensions in facilitating the presence of residual oil, implying that more

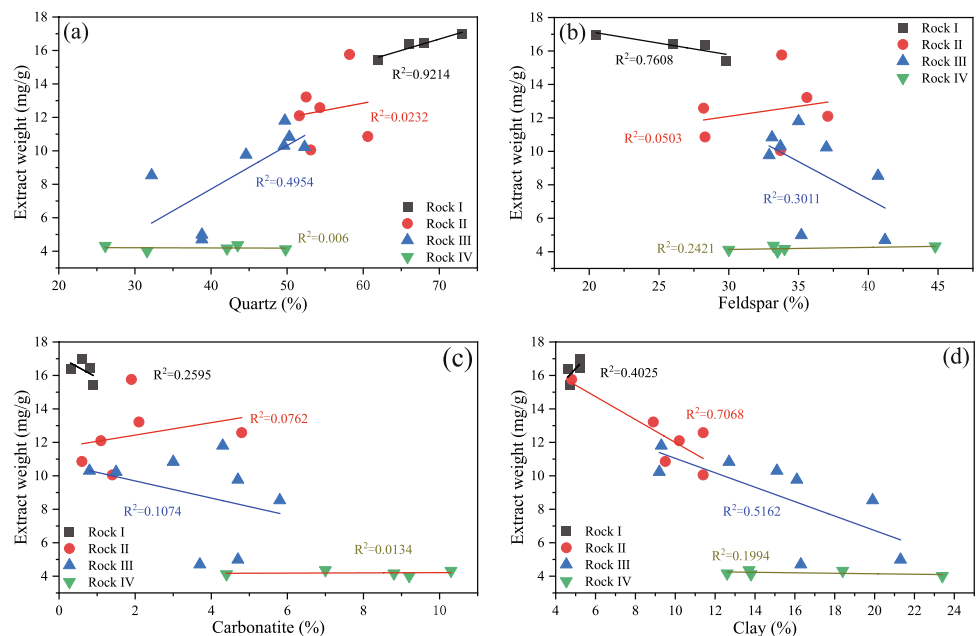
homogeneously sorted reservoirs are likely to harbor greater quantities of residual oil.

Overall, the analysis underscores that reservoirs with larger pore spaces and more favorable pore and throat configurations tend to be more conducive to residual oil accumulation. The marked heterogeneity observed across different tight sandstone reservoir types results in distinct patterns of residual oil distribution, emphasizing the need for tailored recovery strategies that consider the specific pore structure characteristics of each reservoir type.

Effects of mineral composition on the content of residual oil

Minerals lay the groundwork for the reservoir space and pore throat medium, significantly influencing oil–rock interactions and the distribution of crude oil within the reservoir (Zhou et al. 2022b; Zhang et al. 2023). Figure 14 explores the relationship between the extract weight of residual oil and the mineral composition, specifically focusing on quartz, feldspar, carbonatite, and clay minerals. The analysis reveals varying degrees of correlation between these minerals and the presence of residual oil across different reservoir types. (1) Quartz Content: A significant positive correlation between quartz content and residual oil extracts is observed in Rock I and Rock III, with correlation coefficients of 0.9214 and 0.4951, respectively (Fig. 14a). However, in Rock II and Rock IV, quartz content does not show a clear correlation with residual oil extract. Given quartz’s low adsorption capacity toward crude oil (Bahmaninia et al. 2021; Ansari

Fig. 14 Influence of mineral compositions on residual oil distribution across different reservoir types



et al. 2022; Hong et al. 2022), this pattern suggests that residual oil occurrence is less about adsorption and more related to the heavy components' precipitation or deposition within the reservoir spaces (Alimohammadi et al. 2019). (2) Feldspar Content: The relationship between feldspar content and residual oil is complex (Fig. 14b). Rock I shows a significant negative correlation, with a coefficient of 0.7608, indicating that higher feldspar content might lead to reduced residual reservoir space after compaction. Conversely, in Rock II, Rock III, and Rock IV, the correlation between feldspar content and residual oil is minimal. This complexity can be attributed to feldspar's poor anti-compaction properties and the dual role of feldspar dissolution, which, while creating some space for residual oil (Fig. 14e), also affects the overall distribution of residual oil within the reservoir.

These findings highlight the nuanced role of mineral content in influencing the accumulation and distribution of residual oil within tight sandstone reservoirs. The pronounced positive correlation between quartz content and residual oil in certain reservoirs underscores the importance of reservoir space configuration in oil accumulation. Conversely, the negative correlation observed between feldspar content and residual oil in Rock I suggests that factors such as mineral compaction and dissolution dynamics play critical roles in determining the availability of space for oil accumulation.

A negative correlation exists between carbonatite content and the extract weight of residual oil in the Chang 8 Member tight sandstone reservoirs, albeit this correlation is weak across the various reservoir types (Fig. 14c). Carbonatite, an ionic mineral, tends to exhibit positive charges on its surface, which contrasts with the predominantly negative charges carried by crude oil molecules (Li et al. 2018a). Theoretically, this disparity in charges could facilitate crude oil adsorption onto carbonatite surfaces through electrostatic interactions and van der Waals forces, potentially altering the wettability of the carbonatite rock surface (Li et al. 2018a; Bai et al. 2019; Li et al. 2022). However, the observed correlation suggests that the mechanisms governing the presence of residual oil in these reservoirs might extend beyond simple adsorption, potentially involving the precipitation or deposition of asphaltenes through oil–oil interactions (Alimohammadi et al. 2019; Taheri-Shakib et al. 2019a).

Similarly, clay minerals, known for their high specific surface area, have the capacity to adsorb crude oil components, particularly heavy fractions and saturates (Pernyeszi et al. 1998; Pan and Liu 2009; Herawati et al. 2022). The relationship between clay mineral content and residual oil in the Chang 8 Member (Fig. 14d) indicates a significant negative correlation, especially notable in Rock II and Rock III. This pattern implies that while clay minerals are adept

at adsorbing crude oil, their role in the overall distribution of residual oil within these particular reservoir types might be limited. In Rock I, the minimal presence of clay minerals may modify the original seepage patterns within the reservoir, facilitating localized areas of crude oil enrichment (Fig. 6a). On the other hand, Rock IV's significant clay mineral content could lead to the constriction of pore throats, thereby restricting the flow of crude oil and contributing to localized oil accumulation.

These findings highlight the complex interplay between mineral composition and the distribution of residual oil within tight sandstone reservoirs. While certain minerals like carbonatite and clays have the potential to influence crude oil adsorption and seepage patterns, the overall impact on residual oil distribution appears to be governed by a combination of factors, including the physicochemical interactions between oil components and the reservoir rock, as well as the structural characteristics of the pore network.

Enrichment mechanism of residual oil in tight sandstone reservoirs

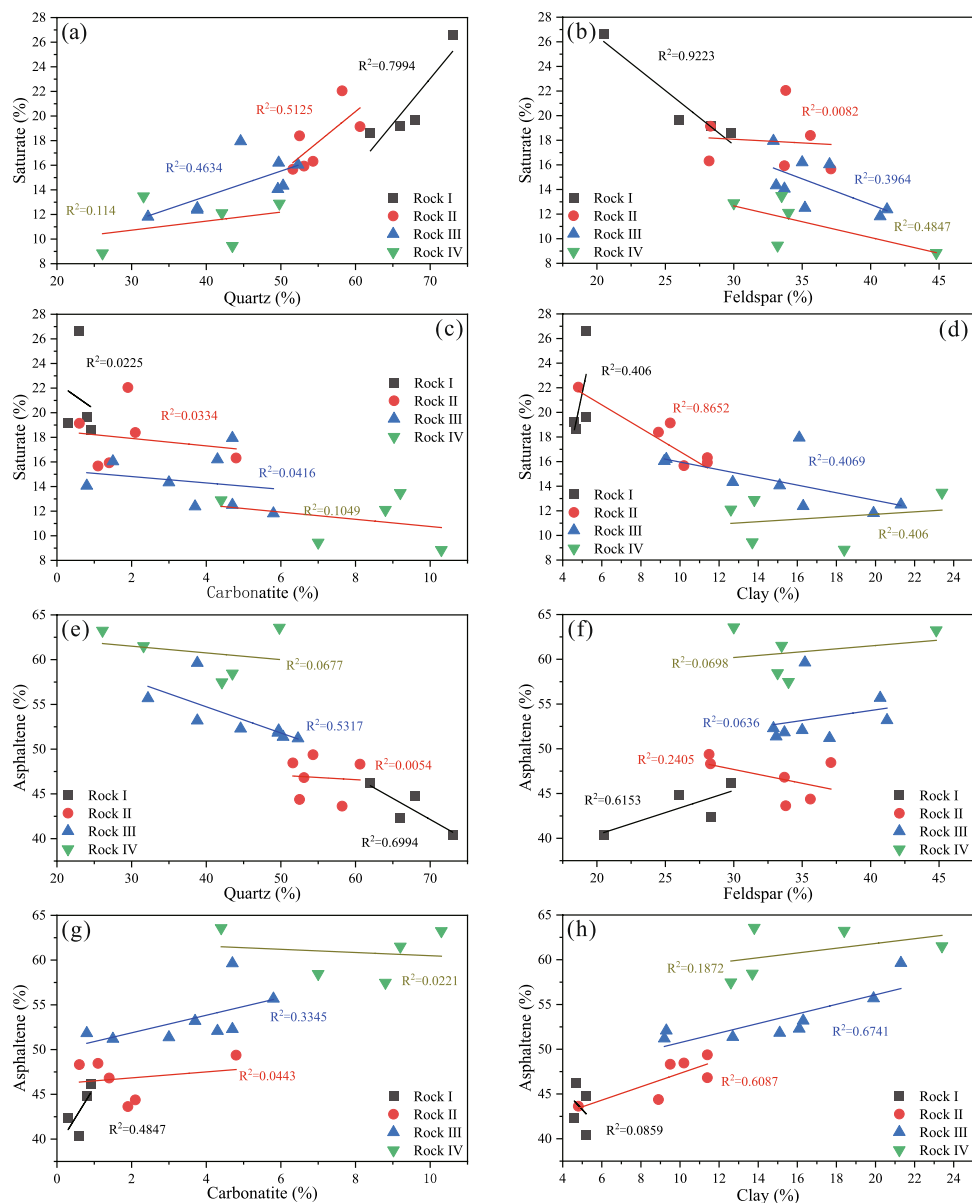
Relationship between mineral composition and oil components

The detailed analysis conducted on the Chang 8 Member tight sandstone reservoirs in the Ordos Basin reveals that the distribution of residual oil is not only influenced by the reservoir's inherent heterogeneity but also by the properties of the crude oil itself. Further investigation into the relationship between oil components and minerals (Fig. 15) has provided insightful revelations about how different minerals interact with the various components of crude oil.

The analysis shows a positive correlation between quartz content and the presence of saturates in the oil (Fig. 15a). This suggests that quartz, being the principal framework mineral in tight sandstone reservoirs, is more associated with the accumulation of lighter crude oil components, such as saturates. Conversely, feldspar, carbonate rocks, and clay minerals exhibit a negative correlation with saturates (Fig. 15b–d). This pattern indicates that these minerals might not favor the retention or accumulation of lighter oil components within the reservoir, potentially due to their specific surface properties or interactions with crude oil.

An interesting inverse trend emerges when examining the relationship between different minerals and asphaltenes, the heavier components of crude oil. There is a negative correlation between quartz content and asphaltenes (Fig. 15e), whereas feldspar, carbonate rocks, and clay minerals show a positive correlation with asphaltenes (Fig. 15f–h). This finding suggests that the latter group of minerals might provide favorable conditions for the accumulation or adsorption of heavier oil components, possibly due to their ability to

Fig. 15 Impact of mineral compositions on oil component distributions of residual oil across different reservoir types



interact more effectively with asphaltenes through various physicochemical mechanisms.

These observations highlight the complex and varied interactions between crude oil components and reservoir minerals, significantly impacting the distribution and accumulation of residual oil within tight sandstone formations. Understanding these nuanced relationships is crucial for tailoring enhanced oil recovery strategies that consider both the heterogeneity of the reservoir and the specific characteristics of the crude oil. By taking into account the differential affinities between oil components and reservoir minerals, recovery efforts can be optimized to target the extraction of both lighter and heavier oil fractions more effectively, potentially improving the overall recovery rates from tight sandstone reservoirs.

The comprehensive analysis conducted on the Chang 8 Member tight sandstone reservoirs in the Ordos Basin reveals insightful correlations between mineral content and crude oil components, significantly influencing the distribution and accumulation of residual oil within the reservoir.

Quartz and Saturates: A strong positive correlation between quartz content and saturates (Fig. 15a) with a correlation coefficient of 0.7994 indicates that higher quartz content enhances saturate enrichment. This is likely due to quartz's limited adsorption capacity for crude oil, particularly for asphaltenes, allowing lighter components like saturates to remain more prevalent in the reservoir. The interaction between oil components, coupled with migration driven by reservoir heterogeneity, further facilitates the enrichment of lighter components.

Quartz and Asphaltenes: The observed negative correlation between quartz content and asphaltenes (Fig. 15e), with a correlation coefficient of 0.6994, suggests that an increase in quartz content within the reservoir tends to reduce asphaltene accumulation, corroborating quartz's role in favoring lighter oil components over heavier ones.

Feldspar's Role: The correlation between feldspar content and saturates (Fig. 15b) and asphaltenes (Fig. 15f) indicates that feldspar promotes asphaltene enrichment while potentially hindering saturate accumulation. This dynamic may be attributed to the increased surface roughness and the creation of small dissolution-induced pores in feldspar, which are conducive to the adsorption and precipitation of asphaltenes, thus impacting the distribution of lighter components.

Carbonate's Influence: The mild negative correlation with saturates and a mild positive correlation with asphaltenes (Fig. 15c,g) suggest carbonate's complex role in crude oil distribution. While disrupting pore throat structures and impeding migration, the positive surface charge of carbonate minerals may still attract negatively charged asphaltenes, affecting the spatial distribution of oil components within the reservoir.

Clay Minerals: The correlation between clay content and saturates/asphaltenes (Fig. 15d, h) highlights clay minerals' capacity to influence the distribution of oil components. The presence of clay can deter saturate distribution while promoting asphaltene enrichment, potentially due to the impact of clay on pore throat space and connectivity, which

amplifies reservoir heterogeneity and affects crude oil migration patterns.

These findings elucidate the intricate relationships between reservoir mineralogy and crude oil components, demonstrating that the distribution of residual oil in tight sandstone reservoirs is a function of both the inherent properties of the reservoir and the complex interplay between minerals and crude oil. The pronounced heterogeneity of these reservoirs leads to varied distributions of oil components across different reservoir types, emphasizing the need for tailored recovery strategies that consider the specific mineralogical and crude oil component interactions within each reservoir.

Enrichment mechanism

Building on the comprehensive analysis of micro-occurrence states of residual oil and its interaction with reservoir types and mineral compositions in the Chang 8 tight sandstone reservoirs of the Ordos Basin, this study proposes a micro-enrichment model for residual oil within tight sandstone formations (Fig. 16).

The genesis of oil and gas in source rocks marks the beginning of a journey that sees these hydrocarbons migrate toward and interact with the reservoir rock. As crude oil moves through the pore throat surfaces of the reservoir, it engages in a series of oil–rock interactions (Taheri-Shakib et al. 2019a, b; Zhou et al. 2023; Zhang et al. 2023). The

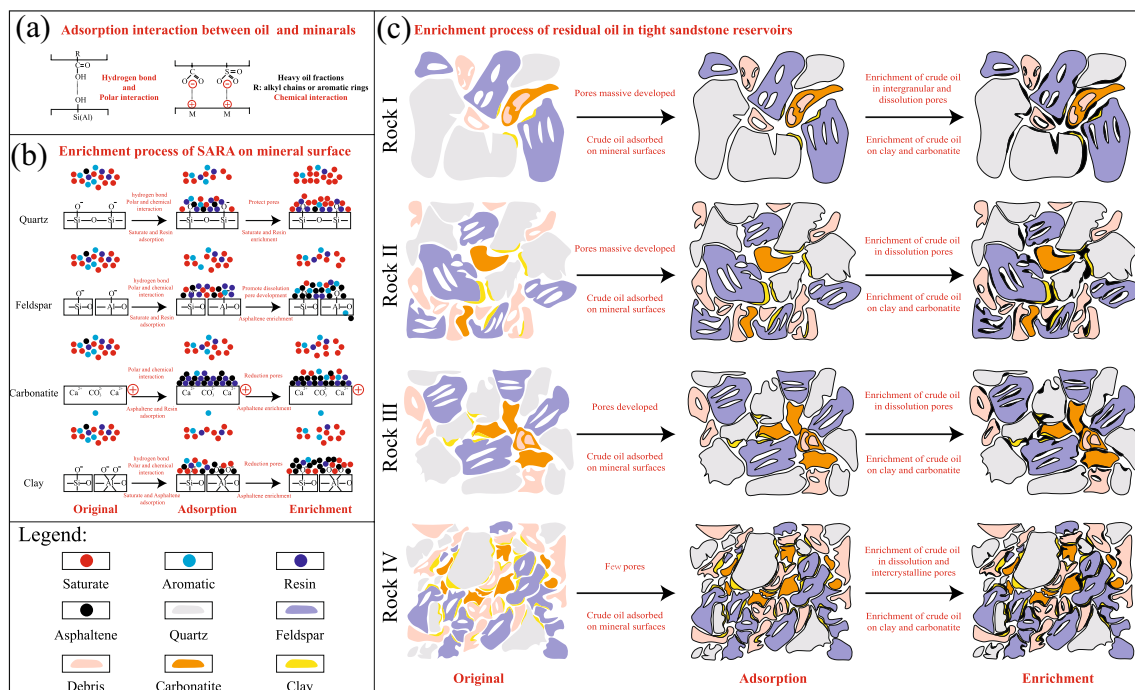


Fig. 16 Schematic illustrations of **a** Adsorption interaction between crude oil and minerals; **b** enrichment process of SARA components on mineral surfaces; **c** enrichment process of residual oil in tight sandstone across different reservoir types

interactions between minerals and crude oil primarily involve physical adsorption mechanisms such as hydrogen bonding, van der Waals forces, and polarity (Fig. 16a), as well as chemical adsorption interactions including metal cation bridging and covalent bonding (Bai et al. 2019; Li et al. 2018b).

In the natural geological setting, minerals like quartz, feldspar, and clay are typically wetted by water due to the aqueous environment under which rock formation occurs. This exposure leads to hydroxylation of the mineral surfaces (Bai et al. 2019). Crude oil contains macromolecules rich in functional groups such as carboxyl, amino, carbonyl, and phenolic hydroxyl groups, which can engage with mineral surfaces through hydrogen bonding, forming an adsorptive layer (Dudášová et al. 2008). This transition from a water-wetted to an oil-wetted mineral surface encourages the self-association of heavy oil components and the adsorption of lighter components (Fig. 16b).

Furthermore, as crude oil infiltrates the reservoir, its lighter components, especially saturates due to their smaller molecular size, tend to migrate preferentially into the primary reservoir spaces. This migration leads to the formation of an adsorption layer between these saturate components and the mineral particles of the sandstone reservoir (Pan and Liu 2009). This selective migration and adsorption process underscores the nuanced dynamics of oil–rock interactions within tight sandstone reservoirs, revealing the complex mechanisms that govern the distribution and accumulation of residual oil. The proposed micro-enrichment model highlights the intricate interplay between crude oil components and reservoir mineralogy, offering insights into the factors that influence the distribution of residual oil within tight sandstone formations.

In the intricate subsurface environment of the Chang 8 Member tight sandstone reservoirs in the Ordos Basin, the micro-occurrence states of residual oil and their responses to reservoir types and mineral compositions have been meticulously examined. This analysis has led to the development of a micro-enrichment model for residual oil, capturing the nuanced dynamics of oil–rock interactions (Fig. 16).

Quartz, with its low cation exchange capacity (CEC), modest specific surface area, and weak adsorption properties toward crude oil, plays a significant role in the enrichment of saturates within the reservoir. The presence of Si–O–Si groups on quartz surfaces facilitates the formation of hydroxyl groups through interaction with water, enabling hydrogen bonding with the polar groups present in crude oil (Fig. 16b). The adsorption of crude oil on quartz surfaces, particularly enhanced by the presence of heteroatoms in non-hydrocarbons and asphaltenes, underscores the complexity of oil–quartz interactions, including π – π stacking. These interactions not only lead to the adsorption of asphaltene

molecules but also facilitate the aggregation of these molecules, enhancing the preservation of pore throat space and promoting oil enrichment (Fig. 14a).

Feldspar, on the other hand, introduces a contrasting dynamic. As a primary aluminosilicate mineral rich in hydroxyl groups, feldspar's surface properties contribute to the adsorption of saturates and resin. However, feldspar's susceptibility to dissolution, particularly in the presence of organic acids, complicates the reservoir's pore throat system. This not only hampers crude oil ingress but also modifies the local concentration of crude oil within dissolution-induced pores, fostering the accumulation of asphaltenes (Fig. 16b).

Carbonatite minerals, particularly those bearing iron, exhibit a strong positive charge that attracts negatively charged groups in tight oil, facilitating the adsorption of polar macromolecules such as resins and asphaltenes. Despite this, the role of carbonatite as a cementing agent during diagenesis can encroach upon pore space, reducing reservoir connectivity and heterogeneity, thus impacting residual oil distribution (Fig. 14c).

Clay minerals, with their high CEC and extensive surface area, exhibit a remarkable capacity for adsorbing crude oil, especially asphaltenes and saturates. The structural flexibility of clay minerals allows for the formation of oil–clay complexes, influencing the distribution and concentration of crude oil within the reservoir. The proliferation of clay can lead to localized variations in crude oil concentration, promoting the deposition of asphaltenes and the formation of residual oil as flake and solid OMA (Fig. 6c).

This study elucidates the profound influence of mineralogy on the micro-occurrence states of residual oil in tight sandstone reservoirs. The interplay between minerals and crude oil components, facilitated by both physical and chemical adsorption mechanisms, dictates the distribution and accumulation patterns of residual oil. Understanding these interactions is crucial for refining oil recovery strategies, highlighting the need for tailored approaches that consider the specific mineralogical and compositional characteristics of tight sandstone reservoirs.

Based on the comprehensive analyses, this study elucidates the enrichment pattern of residual oil across different types of tight sandstone reservoirs within the Chang 8 Member, Ordos Basin (Fig. 16c). The findings underscore the intricate interplay between mineralogical composition, oil–rock interactions, and the physical characteristics of reservoirs in dictating the distribution and accumulation of residual oil.

In Rock I, characterized by a significant presence of quartz, the reservoir demonstrates robust anti-compaction capabilities, facilitating the development of micron-scale pore throat spaces. This structural integrity allows for the formation of an initial adsorption layer by saturates and

asphaltenes on mineral surfaces within the reservoir, notably on carbonate and clay minerals. Following oil–rock interactions, a considerable portion of tight oil remains within Rock I pores, enriched through subsequent oil–oil interactions with the pre-formed adsorption layer. This process is predominantly marked by the enrichment of lighter components, leveraging the earlier adsorption of heavier constituents.

As Rock II and Rock III exhibit increased feldspar content, the development of dissolved feldspar pores alters the original roughness of pores and throats. The charged crude oil forms an adsorbed oil film along the periphery of these pores, while carbonate and clay surfaces absorb significant amounts of crude oil. The reduced pore-throat connectivity in these reservoirs leads to the partial blockage of crude oil flow, resulting in the accumulation of crude oil in semi-closed or closed pores and the formation of solid and flake OMA within intergranular and secondary dissolution pores.

Rock IV reservoirs, with extensive carbonate rocks and clay minerals, are characterized by smaller pore throats, poor connectivity, and pronounced heterogeneity. The traversing crude oil forms adsorption layers on mineral surfaces, particularly carbonate and clay, predominantly comprising heavier components. The flow of crude oil is impeded, leading to its accumulation within the intercrystalline pores and fine throats of clay minerals.

This enrichment process in tight sandstone reservoirs unfolds in two phases: the adsorption stage and the pore throat sealing stage. The adsorption stage, influenced by the reservoir's mineral composition, promotes the adsorption of crude oil, particularly heavy components, on mineral surfaces. Conversely, the pore throat sealing stage, dictated by the dimensions and connectivity of pore throats, enhances the reservoir's capacity for residual oil enrichment. The heterogeneity of tight sandstone reservoirs drives the observed variance in residual oil distribution across reservoir types.

A tiered exploitation strategy is recommended, prioritizing Rock I and Rock II reservoirs for development due to their favorable pore throat connectivity and lighter residual oil composition. Rock III and Rock IV reservoirs, while less conducive to development under current conditions, may serve as potential resources for selective exploitation, contingent upon favorable economic conditions. This nuanced understanding of residual oil enrichment patterns underscores the need for tailored recovery strategies that account for the unique mineralogical and physical characteristics of tight sandstone reservoirs.

Conclusions

The comprehensive examination of the Chang 8 Member tight sandstone reservoirs in the Huaqing area of the Ordos Basin has provided pivotal insights into the characteristics and distribution of residual oil, highlighting the complex interplay of geological and geochemical factors. The reservoirs, primarily composed of feldspathic litharenite and lithic arkose, feature a diverse array of pore types including residual intergranular pores, feldspar dissolved pores, debris dissolved pores, and intercrystalline pores. This diversity underscores the heterogeneity of pore architecture, which is instrumental in dictating fluid dynamics within these formations.

1. Through detailed multi-solvent continuous extraction and oil component analysis, it was discovered that residual oil within these reservoirs predominantly exists as oil-mineral aggregates OMA in three distinct morphologies: droplet-like OMA, solid OMA, and flake OMA. The observed patterns reveal a decrease in residual oil distribution with declining reservoir quality, alongside an increase in the heavy component content of the residual oil. This highlights the critical influence of the original reservoir space size, pore throat connectivity, and the development of the skeletal mineral quartz on residual oil distribution.
2. The initial adsorption phase of crude oil, significantly shaped by mineral-crude oil interactions, sets the stage for subsequent residual oil enrichment processes. These processes are governed by a combination of factors, including oil–oil interactions, the self-aggregation of heavy components, and the occlusion of pore throats by interstitial materials, particularly carbonatite and clay. Together, these elements orchestrate the differential enrichment of residual oil across the reservoir spectrum.
3. The impact of residual oil enrichment on reservoir properties is evident in the notable reductions in pore and throat dimensions, with average reductions in porosity and permeability measured at 2.63% and 0.197 mD, respectively. These changes represent average percentage declines of 27.19% and 46.69% in porosity and permeability, respectively, underscoring the challenges faced in exploiting these tight sandstone reservoirs.

Building upon the comprehensive insights garnered from this study, future research endeavors should aim to further elucidate the molecular mechanisms underpinning the interactions between various crude oil components and tight sandstone minerals, particularly focusing on the role of interstitial substances in modulating oil adsorption and aggregation processes. Additionally, it would be beneficial to

explore advanced recovery techniques tailored to the unique physicochemical landscapes of tight sandstone reservoirs, leveraging the nuanced understanding of pore structure and mineralogy to enhance the efficacy of oil extraction from these complex geological formations.

Acknowledgements The authors extend their appreciation to the Changqing Oil Field for supplying the drill cores employed in this study. We also gratefully acknowledge the insightful suggestions provided by the reviewers from Wuxi Research Institute of Petroleum Geology, Sinopec, which significantly enhanced the quality of this work. Special thanks are conveyed to Prof. Yitian Xiao, whose valuable advice was instrumental in shaping the research.

Author Contributions QZ contributed to writing—original draft, conceptualization, and funding acquisition; JL contributed to resources, validation, and formal analysis; DZ contributed to writing—review and editing, methodology, and validation; CL contributed to resources and investigation; YX contributed to data curation, visualization, and software; GC contributed to supervision and formal analysis; CL contributed to project administration and funding acquisition. All authors have read and agreed to the published version of the manuscript.

Funding This research was supported by the National Natural Science Foundation of China [Grant Nos. 42002175, 42302184, 41975117 and 42050104], the Key Laboratory of Petroleum Resources Research, Gansu Province [Grant No. SZDKFJJ20201210], Science and Technology Fund Program of Gansu Province [Grant Nos. 22JR5RA045, 22JR5RA084], National Key R & D Program of China [Grant No. 2018YFA0702400], and the Science Foundation of SINOPEC Group [Grant No. P21085-6].

Declarations

Conflict of interest The authors declare that they have no known competing financial interests or personal relationships that could have appeared to influence the work reported in this paper.

Open Access This article is licensed under a Creative Commons Attribution 4.0 International License, which permits use, sharing, adaptation, distribution and reproduction in any medium or format, as long as you give appropriate credit to the original author(s) and the source, provide a link to the Creative Commons licence, and indicate if changes were made. The images or other third party material in this article are included in the article's Creative Commons licence, unless indicated otherwise in a credit line to the material. If material is not included in the article's Creative Commons licence and your intended use is not permitted by statutory regulation or exceeds the permitted use, you will need to obtain permission directly from the copyright holder. To view a copy of this licence, visit <http://creativecommons.org/licenses/by/4.0/>.

References

- Alimohammadi S, Zendejboudi S, James L (2019) A comprehensive review of asphaltene deposition in petroleum reservoirs: theory, challenges, and tips. *Fuel* 252:753–791. <https://doi.org/10.1016/j.fuel.2019.03.016>
- Ansari S, Bahmaninia H, Mohammadi MR et al (2022) On the evaluation of asphaltene adsorption onto dolomite surface: the roles of flow condition, composition of asphaltene, and dolomite size. *Alexandria Eng J* 61(12):9411–9425. <https://doi.org/10.1016/j.aej.2022.02.066>
- Baban A, Keshavarz A, Amin R et al (2023) Residual trapping of CO₂ and enhanced oil recovery in oil-wet sandstone core—a three-phase pore-scale analysis using NMR. *Fuel* 332:126000. <https://doi.org/10.1016/j.fuel.2022.126000>
- Bahmaninia H, Ansari S, Mohammadi MR et al (2021) Toward mechanistic understanding of asphaltene adsorption onto quartz surface: the roles of size, concentration, and hydrophobicity of quartz, asphaltene composition, flow condition, and aqueous phase. *J Petrol Sci Eng* 205:108820. <https://doi.org/10.1016/j.petrol.2021.108820>
- Bai Y, Sui H, Liu X et al (2019) Effects of the n, o, and s heteroatoms on the adsorption and desorption of asphaltenes on silica surface: a molecular dynamics simulation. *Fuel* 240:252–261. <https://doi.org/10.1016/j.fuel.2018.11.135>
- Baoquan M, Shumin C, Weilin Y et al (2021) Pore structure evaluation of low permeability clastic reservoirs based on sedimentation diagenesis: a case study of the Chang 8 reservoirs in the Shenbei region, Ordos basin. *J Petrol Sci Eng* 196:107841. <https://doi.org/10.1016/j.petrol.2020.107841>
- Bolouri SH, Ghoojani E (2012) Permeability impairment study due to asphaltene deposition: experimental and modeling approach. *Transp Porous Media* 91(3):999–1012. <https://doi.org/10.1007/s11242-011-9887-6>
- Cai C, Li K, Zhu Y et al (2010) TSR origin of sulfur in Permian and triassic reservoir bitumen, east Sichuan basin, China. *Organ Geochem* 41(9):871–878. <https://doi.org/10.1016/j.orggeochem.2010.03.009>
- Davudov D, Moghanloo RG (2019) A new model for permeability impairment due to asphaltene deposition. *Fuel* 235:239–248. <https://doi.org/10.1016/j.fuel.2018.07.079>
- Dudášová D, Simon S, Hemmingsen PV et al (2008) Study of asphaltene adsorption onto different minerals and clays. *Colloids Surf A* 317(1–3):1–9. <https://doi.org/10.1016/j.colsurfa.2007.09.023>
- Er C, Zhao J, Li Y et al (2022) Relationship between tight reservoir diagenesis and hydrocarbon accumulation: an example from the early Cretaceous Fuyu reservoir in the Daqing oil field, Songliao basin, China. *J Petrol Sci Eng* 208:109422. <https://doi.org/10.1016/j.petrol.2021.109422>
- Gong Y, Liu S, Zhu R et al (2015) Micro-occurrence of Cretaceous tight oil in southern Songliao basin, NE China. *Pet Explor Dev* 42(3):323–328. [https://doi.org/10.1016/S1876-3804\(15\)30022-7](https://doi.org/10.1016/S1876-3804(15)30022-7)
- Guo Q, Yao Y, Hou L et al (2022) Oil migration, retention, and differential accumulation in sandwiched lacustrine shale oil systems from the Chang 7 member of the upper Triassic Yanchang formation, Ordos basin, China. *Int J Coal Geol* 261:104077. <https://doi.org/10.1016/j.coal.2022.104077>
- Hematfar V, Maini B, Chen Z (2018) Experimental investigation of asphaltene adsorption in porous media due to solvent injection and effects on relative permeability. *Int J Multiphase Flow* 99:174–185. <https://doi.org/10.1016/j.ijmultiphaseflow.2017.10.005>
- Herawati I, Permadi P, Rochliadi A et al (2022) Adsorption of anionic surfactant on sandstone reservoir containing clay minerals and its effect on wettability alteration. *Energy Rep* 8:11554–11568. <https://doi.org/10.1016/j.egy.2022.08.268>
- Hong X, Yu H, Xu H et al (2022) Competitive adsorption of asphaltene and n-heptane on quartz surfaces and its effect on crude oil transport through nanopores. *J Mol Liq* 359:119312. <https://doi.org/10.1016/j.molliq.2022.119312>
- Huang H, Li R, Chen W et al (2021) Revisiting movable fluid space in tight fine-grained reservoirs: a case study from Shahejie shale in the Bohai Bay Basin, NE China. *J Petrol Sci Eng* 207:109170. <https://doi.org/10.1016/j.petrol.2021.109170>

- Huangfu Y, Zhang J, Zhang S et al (2022) Characteristics of shale oil in different occurrence states of cretaceous Gingshankou formation in the northern Songliao Basin. *Acta Geol Sin* 96:1–16. <https://doi.org/10.19762/j.cnki.dizhixuebao.2022228>
- Jin L, Jian W, Baozhen Z et al (2022) In situ occurrence of shale oil in micro-nano pores in Permian Lucaogou formation in Jimsar Sag, Junggar basin. *Petrol Geol Exp* 44(2):270–278. <https://doi.org/10.11781/sydz202202270>
- Lai J, Wang G, Wang Z et al (2018) A review on pore structure characterization in tight sandstones. *Earth Sci Rev* 177:436–457. <https://doi.org/10.1016/j.earscirev.2017.12.003>
- Li S, Liu Y, Xue L et al (2022) A molecular insight into the effect of key ions on the detachment of crude oil from calcite surface: implication for low salinity water flooding in carbonate reservoirs. *J Petrol Sci Eng* 208:109562. <https://doi.org/10.1016/j.petrol.2021.109562>
- Li X, Bai Y, Sui H et al (2018) Understanding desorption of oil fractions from mineral surfaces. *Fuel* 232:257–266. <https://doi.org/10.1016/j.fuel.2018.05.112>
- Li Z, Wu S, Xia D et al (2018) An investigation into pore structure and petrophysical property in tight sandstones: a case of the Yanchang formation in the Southern Ordos Basin, China. *Mar Pet Geol* 97:390–406. <https://doi.org/10.1016/j.marpetgeo.2018.07.014>
- Liu H, Luo Y, Meng Y et al (2021) Effects of pore structure on the moveable oil saturation in water-driven tight oil sandstone reservoirs. *J Petrol Sci Eng* 207:109142. <https://doi.org/10.1016/j.petrol.2021.109142>
- Menhui Q, Qigui J, Maowen L et al (2017) Quantitative characterization of extractable organic matter in lacustrine shale with different occurrences. *Petrol Geol Exp* 39(2):278–286. <https://doi.org/10.11781/sydz201702278>
- Menhui Q, Qigui J, Maowen LI et al (2020) Three-dimensional quantitative fluorescence analysis and application in shale. *Petrol Geol Exp* 42(2):311–318. <https://doi.org/10.11781/sydz202002311>
- Mohammed I, Mahmoud M, Al Shehri D et al (2021) Asphaltene precipitation and deposition: a critical review. *J Petrol Sci Eng* 197:107956. <https://doi.org/10.1016/j.petrol.2020.107956>
- Pan C, Liu D (2009) Molecular correlation of free oil, adsorbed oil and inclusion oil of reservoir rocks in the Tazhong uplift of the Tarim Basin, China. *Org Geochem* 40(3):387–399. <https://doi.org/10.1016/j.orggeochem.2008.11.005>
- Pang X, Wang G, Kuang L et al (2022) Insights into the pore structure and oil mobility in fine-grained sedimentary rocks: The Lucaogou formation in Jimusar Sag, Junggar Basin, China. *Mar Pet Geol* 137:105492. <https://doi.org/10.1016/j.marpetgeo.2021.105492>
- Perneszi T, Patzkó Á, Berkesi O et al (1998) Asphaltene adsorption on clays and crude oil reservoir rocks. *Colloids Surf A* 137(1–3):373–384. [https://doi.org/10.1016/S0927-7757\(98\)00214-3](https://doi.org/10.1016/S0927-7757(98)00214-3)
- Qiao J, Zeng J, Jiang S et al (2020) Impacts of sedimentology and diagenesis on pore structure and reservoir quality in tight oil sandstone reservoirs: implications for macroscopic and microscopic heterogeneities. *Mar Pet Geol* 111:279–300. <https://doi.org/10.1016/j.marpetgeo.2019.08.008>
- Qu Y, Sun W, Wu H et al (2022) Impacts of pore-throat spaces on movable fluid: implications for understanding the tight oil exploitation process. *Mar Pet Geol* 137:105509. <https://doi.org/10.1016/j.marpetgeo.2021.105509>
- Ren D, Wang X, Kou Z et al (2023) Feasibility evaluation of CO₂ EOR and storage in tight oil reservoirs: A demonstration project in the Ordos Basin. *Fuel* 331:125652. <https://doi.org/10.1016/j.fuel.2022.125652>
- Song X, Gao H, Feng C et al (2023) Analysis of the influence of micro-pore structure on oil occurrence using nano-CT scanning and nuclear magnetic resonance technology: an example from Chang 8 tight sandstone reservoir, Jiyuan, Ordos Basin. *Processes* 11(4):1127. <https://doi.org/10.3390/pr11041127>
- Song Y, Song Z, Zhang Y et al (2022) Pore scale performance evaluation and impact factors in nitrogen huff-n-puff EOR for tight oil. *Pet Sci* 19(6):2932–2940. <https://doi.org/10.1016/j.petsci.2022.05.012>
- Strelets LA, Ilyin SO (2021) Effect of enhanced oil recovery on the composition and rheological properties of heavy crude oil. *J Petrol Sci Eng* 203:108641. <https://doi.org/10.1016/j.petrol.2021.108641>
- Sun L, Zou C, Jia A et al (2019) Development characteristics and orientation of tight oil and gas in china. *Pet Explor Dev* 46(6):1073–1087. [https://doi.org/10.1016/S1876-3804\(19\)60264-8](https://doi.org/10.1016/S1876-3804(19)60264-8)
- Taheri-Shakib J, Rajabi-Kochi M, Kazemzadeh E et al (2018) A comprehensive study of asphaltene fractionation based on adsorption onto calcite, dolomite and sandstone. *J Petrol Sci Eng* 171:863–878. <https://doi.org/10.1016/j.petrol.2018.08.024>
- Taheri-Shakib J, Hosseini SA, Kazemzadeh E et al (2019a) Experimental and mathematical model evaluation of asphaltene fractionation based on adsorption in porous media: dolomite reservoir rock. *Fuel* 245:570–585. <https://doi.org/10.1016/j.fuel.2019.02.057>
- Taheri-Shakib J, Keshavarz V, Kazemzadeh E et al (2019b) Experimental and mathematical model evaluation of asphaltene fractionation based on adsorption in porous media: Part 1. Calcite reservoir rock. *J Petrol Sci Eng* 177:24–40. <https://doi.org/10.1016/j.petrol.2019.02.032>
- Wang R, Chi Y, Zhang L et al (2018) Comparative studies of microscopic pore throat characteristics of unconventional super-low permeability sandstone reservoirs: examples of Chang 6 and Chang 8 reservoirs of Yanchang formation in Ordos Basin, china. *J Petrol Sci Eng* 160:72–90. <https://doi.org/10.1016/j.petrol.2017.10.030>
- Wang R, Shi W, Xie X et al (2020a) Clay mineral content, type, and their effects on pore throat structure and reservoir properties: insight from the Permian tight sandstones in the Hangjinqi Area, North Ordos Basin, China. *Mar Pet Geol* 115:104281. <https://doi.org/10.1016/j.marpetgeo.2020.104281>
- Wang Y, Chang X, Sun Y et al (2020b) Investigation of fluid inclusion and oil geochemistry to delineate the charging history of upper Triassic Chang 6, Chang 8, and Chang 9 tight oil reservoirs, Southeastern Ordos Basin, China. *Mar Pet Geol* 113:104115. <https://doi.org/10.1016/j.marpetgeo.2019.104115>
- Xi K, Cao Y, Liu K et al (2019) Authigenic minerals related to wettability and their impacts on oil accumulation in tight sandstone reservoirs: an example from the lower cretaceous Guantou formation in the southern Songliao Basin, China. *J Asian Earth Sci* 178:173–192. <https://doi.org/10.1016/j.jseaes.2018.04.025>
- Xu Y, Lun Z, Pan Z et al (2022) Occurrence space and state of shale oil: a review. *J Petrol Sci Eng* 211:110183. <https://doi.org/10.1016/j.petrol.2022.110183>
- Yang H, Liang X, Niu X et al (2017) Geological conditions for continental tight oil formation and the main controlling factors for the enrichment: a case of Chang 7 member, Triassic Yanchang formation, Ordos Basin, NW China. *Pet Explor Dev* 44(1):11–19. [https://doi.org/10.1016/S1876-3804\(17\)30003-4](https://doi.org/10.1016/S1876-3804(17)30003-4)
- Yang S, Li X, Zhang K et al (2022) The coupling effects of pore structure and rock mineralogy on the pre-Darcy behaviors in tight sandstone and shale. *J Petrol Sci Eng* 218:110945. <https://doi.org/10.1016/j.petrol.2022.110945>
- Yang T, Cao Y, Wang Y et al (2019) Determining permeability cut-off values for net pay study of a low-permeability clastic reservoir: a case study of the Dongying Sag, Eastern China. *J Petrol Sci Eng* 178:262–271. <https://doi.org/10.1016/j.petrol.2019.03.030>

- Yang YB, Xiao WL, Zheng LL et al (2023) Pore throat structure heterogeneity and its effect on gas-phase seepage capacity in tight sandstone reservoirs: a case study from the triassic Yanchang formation, Ordos Basin. *Pet Sci* 20(5):2892–2907. <https://doi.org/10.1016/j.petsci.2023.03.020>
- Yao J, Deng X, Zhao Y et al (2013) Characteristics of tight oil in triassic Yanchang formation, Ordos Basin. *Pet Explor Dev* 40(2):161–169. [https://doi.org/10.1016/S1876-3804\(13\)60019-1](https://doi.org/10.1016/S1876-3804(13)60019-1)
- Zhang D, Han M, Zhou Q et al (2023) The micro-occurrence mechanisms of tight oil: fluid–rock interactions at microscale pores, nanoscale pores, and mineral surfaces. *Energies* 16(9):3917. <https://doi.org/10.3390/en16093917>
- Zhang L, Bao Y, Li J et al (2014) Movability of lacustrine shale oil: a case study of Dongying Sag, Jiyang depression, Bohai bay basin. *Pet Explor Dev* 41(6):703–711. [https://doi.org/10.1016/S1876-3804\(14\)60084-7](https://doi.org/10.1016/S1876-3804(14)60084-7)
- Zhang Q, Liu Y, Wang B et al (2022) Effects of pore-throat structures on the fluid mobility in Chang 7 tight sandstone reservoirs of Longdong area, Ordos Basin. *Mar Pet Geol* 135:105407. <https://doi.org/10.1016/j.marpetgeo.2021.105407>
- Zhengming Y, Yingzhi Z, Mingqiang H et al (2006) Comprehensive evaluation of reservoir in low-permeability oilfields. *Acta Petrolei Sinica* 27(2):64. <https://doi.org/10.7623/syxb200602013>
- Zhou Q, Li C, Chen G et al (2021) The formation mechanism of authigenic chlorite in tight sandstone and its effect on tight oil adsorption during hydrocarbon filling. *Oil Gas Sci Technol Revue d'IFP Energies nouvelles* 76:39. <https://doi.org/10.2516/ogst/2021015>
- Zhou Q, Li X, Qian Z et al (2022a) The occurrence of adsorbed tight oil and its effect on porosity and permeability reduction of triassic lacustrine sandstone reservoir. *Geofluids* 2022:1–16. <https://doi.org/10.1155/2022/6923449>
- Zhou Q, Zhang D, Li X et al (2022b) Insight into the desorption behavior and mechanism of tight oil with in-situ low-temperature thermal. *J Petrol Sci Eng* 218:111001. <https://doi.org/10.1016/j.petrol.2022.111001>
- Zhou Q, Zhang D, Xi M et al (2023) Insights into the effect of micropore structure and mineralogy on adsorbed tight oil in the Huaqing Area, Ordos Basin, China. *Geofluids* 2023:e6065230. <https://doi.org/10.1155/2023/6065230>

Publisher's Note Springer Nature remains neutral with regard to jurisdictional claims in published maps and institutional affiliations.